Translational Oncology
www.transonc.com

Volume 11 Number 2 April 2018 pp. 450–466 450

Preclinical Analysis of JAA-F11, a Specific Anti–Thomsen-Friedenreich Antibody via Immunohistochemistry and *In Vivo* Imaging

Loukia G. Karacosta[*,1], John C. Fisk[*,1], Joseph Jessee[*], Swetha Tati[*], Bradley Turner[†], Diala Ghazal[*], Rachel Ludwig[*], Holly Johnson[*], Julia Adams[‡], Munawwar Sajjad[§], Steven Koury[‡], Rene Roy[¶], James R. Olson[*,#] and Kate Rittenhouse-Olson[*,‡]

[*]For-Robin, Inc, Buffalo, NY; [†]Department of Pathology, University of Rochester, Rochester, NY; [‡]Department of Biotechnical and Clinical Laboratory Sciences, University at Buffalo, Buffalo, NY; [§]Department of Nuclear Medicine, University at Buffalo, Buffalo, NY; [¶]Glycovax Pharma Inc., Montreal, Quebec, Canada; [#]Department of Pharmacology and Toxicology, University at Buffalo, Buffalo, NY

Abstract

The tumor specificity of JAA-F11, a novel monoclonal antibody specific for the Thomsen-Friedenreich cancer antigen (TF-Ag-alpha linked), has been comprehensively studied by *in vitro* immunohistochemical (IHC) staining of human tumor and normal tissue microarrays and *in vivo* biodistribution and imaging by micro-positron emission tomography imaging in breast and lung tumor models in mice. The IHC analysis detailed herein is the comprehensive biological analysis of the tumor specificity of JAA-F11 antibody performed as JAA-F11 is progressing towards preclinical safety testing and clinical trials. Wide tumor reactivity of JAA-F11, relative to the matched mouse IgG_3 (control), was observed in 85% of 1269 cases of breast, lung, prostate, colon, bladder, and ovarian cancer. Staining on tissues from breast cancer cases was similar regardless of hormonal or Her2 status, and this is particularly important in finding a target on the currently untargetable triple-negative breast cancer subtype. Humanization of JAA-F11 was recently carried out as explained in a companion paper "Humanization of JAA-F11, a Highly Specific Anti–Thomsen-Friedenreich Pancarcinoma Antibody and *In Vitro* Efficacy Analysis" (*Neoplasia* 19: 716-733, 2017), and it was confirmed that humanization did not affect chemical specificity. IHC studies with humanized JAA-F11 showed similar binding to human breast tumor tissues. *In vivo* imaging and biodistribution studies in a mouse syngeneic breast cancer model and in a mouse-human xenograft lung cancer model with humanized ^{124}I- JAA-F11 construct confirmed *in vitro* tumor reactivity and specificity. In conclusion, the tumor reactivity of JAA-F11 supports the continued development of JAA-F11 as a targeted cancer therapeutic for multiple cancers, including those with unmet need.

Translational Oncology (2018) 11, 450–466

Introduction

The Thomsen-Friedenreich pancarcinoma antigen (TF-Ag) has long been established as a cancer-associated carbohydrate moiety, with cell surface expression on cancers including those of the breast, colon, prostate, bladder, and ovary [1–8]. Alterations in glycosylation in malignant cells lead to the elevated surface expression of TF-Ag, which is normally cryptic due to glycan chain extensions [5,9,10]. Being tumor restricted and having a role in metastasis, TF-Ag is

Address all correspondence to: Kate Rittenhouse-Olson, For-Robin, Inc, Buffalo, NY.
E-mail: krolson@buffalo.edu
[1]Co-first authors.
Received 17 August 2017; Revised 10 January 2018; Accepted 16 January 2018

1936-5233/18
https://doi.org/10.1016/j.tranon.2018.01.008

considered to be a promising molecule for cancer immunotherapy [8,11–19]. However, previous attempts at therapy directed to this target have been limited due to specificity problems. The glycotope structure of TF-Ag (Galβ-3GalNAc-alpha) has been historically detected and extensively studied with anti-TF sera as well as lectins, primarily peanut agglutinin (PNA) [6,20–25]. However, PNA is not exclusively specific for the TF-Ag glycotope due to its ability to bind to terminal galactosyl residues on many commonly occurring glycoproteins and glycolipids. PNA cannot distinguish between the two TF-Ag anomeric linkage configurations, one of which is linked in an alpha (α) orientation (which is O-linked to serine/threonine residues and is the cancer associated form) from the beta (β) orientation (which is primarily linked to glycolipids on the surface of normal cells) [24,26,27]. Due to the status of TF-Ag as a cancer marker, many polyclonal as well as monoclonal antibodies have been developed towards the TF-Ag disaccharide [24,28–33]. However, although most of these agents were in agreement for the pancarcinoma expression of TF-Ag [2,8,34,35], they were disparate concerning normal tissue staining patterns [23,24,27,29,36]. This could be attributed to specificity issues towards the disaccharide's linkage configuration (alpha vs beta), technical issues involving the loss of sialylation on normal tissues, and the loss of Galβ1-3GalNAc immunoreactivity on cancer tissues created by tissue handling procedures [23,24]. Recently, the chemical specificity of humanized forms of JAA-F11 has been characterized. JAA-F11 was humanized to an IgG_1 in a manner which 1) retained the tumor-associated Galb1-3GalNAc alpha specificity, 2) added antibody-dependent cellular cytotoxicity activity, and 3) retained the ability to internalize for use as an antibody drug conjugate and added *in vivo* efficacy against a human triple-negative breast cancer xenograft [37]. These promising preclinical data are helping move JAA-F11 towards clinical trials, thus increasing the importance of these immunohistochemical (IHC) and imaging studies.

To validate the clinical applicability of JAA-F11, the main objective of this investigation was to immunohistochemically confirm JAA-F11's reported specificity when tested against a large number of various human cancer and normal tissue arrays. A significant shortcoming to a comprehensive study of human tissue is that a human antibody will create considerable background in indirect detection methods using a secondary labeled anti-human IgG antibody due to the presence of human IgG in human tumor and normal tissue samples. Therefore, mouse JAA-F11 was largely used to screen multiple human cancer arrays due to concern regarding this background issue. Nonetheless, a humanized variant of JAA-F11 (hJAA-F11) is most favorable for future therapeutic studies. To circumvent background issues with anti-human immunoglobulin, a biotinylated form of the hJAA-F11, H2aL2a, was used to confirm the mouse JAA-F11 findings. Furthermore, the radiolabeled hJAA-F11 construct, H2aL2a, also showed high specificity for tumor binding in several *in vivo* mouse tumor models. Overall, our results support that the JAA-F11 antibody and specifically its humanized derivative are strong candidates for future human therapeutic studies on a wide array of human carcinomas.

Materials and Methods

Immunohistochemistry

All human tissue array slides were purchased from US Biomax (Rockville, MD). The standard procedure at US Biomax for cancer tissues is to place tumor tissue in neutral pH buffer formalin 15 to 30 minutes after surgical resection for a 24-hour period. Previous data in our lab have shown that fixation for longer than 24 hours results in a loss of TF-Ag reactivity (data not shown), so the US Biomax cancer tumor tissue protocol is optimal for this work. Different criteria are of necessity used for obtaining normal tissue, as these were for the most part obtained during autopsy. Autopsy can begin up to 6 hours after death and can take up to 6 hours, so the normal tissue may remain unresected up to 12 hours [38] after death before being placed into formalin; thus, some effects of *in situ* degradation may be observed on these tissues as opposed to tumor tissue. After fixation, tissues are then placed into ethanol, followed by xylene and then paraffin. To process the slides for IHC, slides were deparaffinized by passing them through xylene and then rehydrated through 100% ethanol, 95% ethanol, 70% ethanol, and finally water. Slides were then subjected to antigen retrieval to expose cross-linked antigen using citrate buffer [10 mM sodium citrate (pH 6.0), 0.5% Tween-20] for 40 minutes in a vegetable steamer, followed by a 20-minute cool-down. Slides were washed twice with Tris-phosphate wash buffer, and endogenous peroxidases were blocked with 3% hydrogen peroxide in methanol for 15 minutes. After another wash step, endogenous biotin was blocked with an avidin-biotin blocking kit (Thermo Scientific, Waltham, MA). Following blocking with a goat sera block (Vector Labs, Burlingame, CA), slides were incubated with either control mouse IgG_3 (Southern Biotech, Birmingham, AL) or JAA-F11 at 25 μg/ml final concentration in goat serum for 1.5 hours. As mouse IgG_3 is prone to self-aggregation, some preparations of JAA-F11 were used that were partially purified only, thus containing a significant portion of bovine serum albumin (BSA) derived from media serum and retained during the antibody purification. For these preparations, the total amount of JAA-F11 was determined using SDS-PAGE and densitometry, so the total amount of applied JAA-F11 was always kept at 25 μg/mL final. Slides were washed and then incubated with biotinylated anti-mouse IgG antibody (Vector Labs, Burlingame, CA) for 30 minutes. Following washing, slides were treated using a Vectastain Elite ABC reagent (Vector Labs, Burlingame, CA) for 30 minutes, then washed and developed with ImmPact DAB chromagen (Vector Labs, Burlingame, CA). Slides were counterstained with Modified Harris Hematoxylin (Richard-Allan Scientific), dehydrated, and then mounted. Slides were scored as 0, 0.5, +1, +1.5, +2, +2.5, or +3 in a microscope (Zeiss) while viewing at 100×. A positive score was one in which after subtraction of the IgG_3 control from the JAA-F11 score, the value was ≥1. Slides were scanned and images taken using an Aperio Scan Scope GL (Leica BioSystems). For IHC using biotinylated human antibodies, primary antibodies were used at 50 μg/ml, an increase needed due to the absence of amplifying secondary antibody, with other steps remaining the same.

Some slides had tissue cores that represented duplications previously tested on a different slide from the same patient's tumor. Replicate specimens were tabulated in the percentages only one time. The screening of the tumor slides was verified using concordance for scoring of these replicates in breast, colon, bladder, prostate, and ovary arrays. The frequency of concordant scores was calculated by analysis of duplicate, triplicate, or higher cases read by a scientist blinded to the presence of tissues from the same case in the different arrays. To tabulate the total score and the positive concordance score, if greater than 50% of sections were blindly scored as positive for staining, then a positive score for this tumor was recorded; otherwise, the patient's tumor was considered negative. In the case of equal

Table 1. Total Positive Staining of All Human Cancer Tissue Types by JAA-F11

Carcinoma Reactivity with JAA-F11			
Cancer Type	# Positive	# of Cases	% Positive
Breast	391 *	444 *	88%
Prostate	70	75	93%
Lung	197 *	235 *	84%
Colon	37	46	80%
Bladder	71	79	90%
Ovary	315	390	81%
total	1081	1269	85%

Immunohistochemically stained tissue arrays were scored as positive as detailed in Materials and Methods.

* For breast and lung cancers, both the original tumor and the metastatic site were counted as separate tumors, as several tissue arrays represented both types of tumors from the same patient.

numbers of positive and negative staining, then the case was removed from the percentage positive analysis. The agreement of positive concordance from organ to organ was comparable, and the overall total average agreement of the scores for all replicate cases from the overlaps was 89%. This verifies the validity of the scoring methodology, as well as the consistent judgment and scoring of the reader, who was blinded to the presence of the replicates.

To further validate scoring, a pathologist served as an independent second reader and scored 863/1269 of the cores. The pathologist remained blinded to the initial reader's score until after his scoring. The pathologist's scores showed agreement with the principle scorer, with a 93.2% correlation of slides being scored positive or negative in agreement (Supplemental File 2).

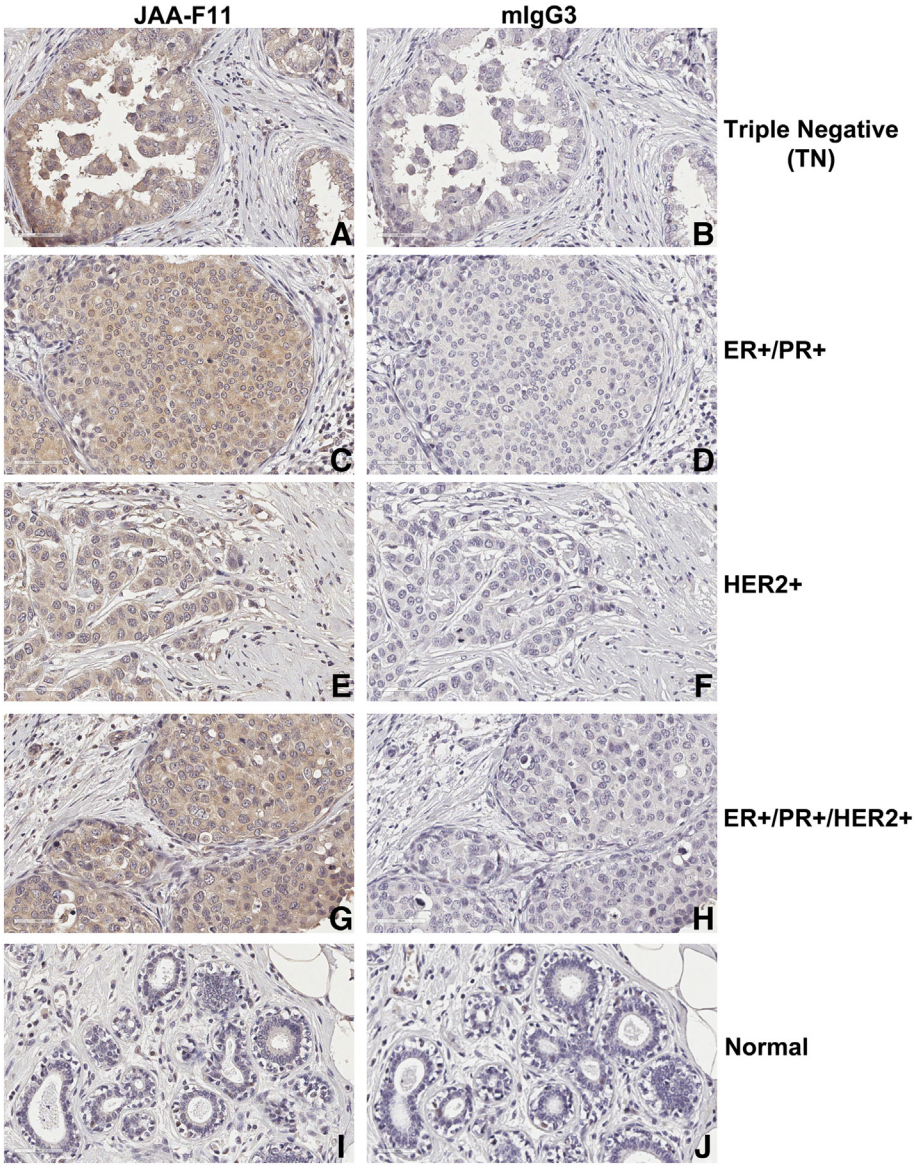

Figure 1. Representative images of human breast cancer staining with JAA-F11 antibody. JAA-F11 staining specificity (left) compared to matched isotype mouse IgG_3 ($mIgG_3$) control (right). Staining is shown for typed breast cancer markers: lacking the three common markers (triple negative, TN) (A, B), positive for ER and PR (ER+/PR+) (C, D), positive for HER2 (HER2+) (E, F), positive for all three markers (ER+/PR+/HER2+) (G, H), and normal breast tissue (I, J). Histological typing into the ER/PR/HER2 groups was provided by US Biomax**.** Magnification: 40×.

Table 2. Positive JAA-F11 Staining in Specific Cases of Human Breast Cancer Samples

(A)

JAA-F11 Reactivity with Breast Cancer: ER, PR, & HER2 Subtypes

Type	#Positive	#Cases	% Positive
Triple negative	118	126	94%
ER+ PR+	56	62	90%
ER+ PR–	23	25	92%
PR+ ER–	19	19	100%
HER2+	80	82	98%

(B)

JAA-F11 Reactivity with Breast Cancer by Stage

Stage	# Positive	# of Cases	% Positive
I	15	20	75%
II	206	238	87%
III	69	76	91%
IV	3	3	100%

(C)

JAA-F11 Reactivity of Breast Tumors and Matching Lymph Nodes

Type	# Positive	# Of Cases	% Positive
Tumors	44	46	96%
Lymph nodes	42	46	91%

(A) Positive JAA-F11 Staining in Breast Cancer Cases Broken Down into Type Based on Overexpression of Specific Cellular Receptors. (B) Staining of Breast Cancer Samples Based on Progressive Staging of the Breast Cancer Case. (C) Staining of Breast Cancer Tumor in Patients That Also Had Metastasis to Lymph Nodes.

Preincubation IHC with Soluble TF-Ag-BSA for Inhibition of TF-Ag Specific Staining. For analysis of the specificity of the staining observed, IHC was performed as above with the following modifications. One hour prior to addition of primary antibody to tissue samples, JAA-F11 at 25 μg/ml was preincubated with either IHC grade BSA (control) or TF-Ag-BSA (100-200 μg/ml) (inhibited) for 1 hour at room temperature. Specific inhibition of JAA-F11 binding to TF-Ag was confirmed using the preincubated JAA-F11 in enzyme-linked immunosorbent assays (ELISAs) against immobilized TF-Ag-BSA where it was found to be decreased ≥75% compared to the BSA addition control. Preincubated JAA-F11 was then used in IHC experiments as detailed before. The amount of inhibition of staining was then graded against the BSA control, and the tissue was considered inhibited for JAA-F11 staining if the change in staining was ≥1. These inhibition scores are presented in Supplemental File 3 and tabulated in Table 4b and c.

Preparation and Biotinylation of hJAA-F11 H2aL2a. The characterization of the hJAA-F11 H2aL2a has been detailed elsewhere [37]. Briefly, two vectors, encoding the heavy and light chains of H2aL2a, were transfected into the Chinese hamster ovary cell line CHO-K1 (ATCC, Manassas, VA). Stable cell lines expressing hJAA-F11 H2aL2a were selected using G418 and histidinol and confirmed to bind to immobilized TF-Ag-α linked to BSA in an enzyme immunoassay [17,39]. hJAA-F11 H2aL2a was then purified using rProtein A Sepharose Fast Flow resin (GE Healthcare, Pittsburgh, PA), followed by Capto S ImpAct resin (GE Healthcare, Pittsburgh, PA).

Purified hJAA-F11 H2aL2a was dialyzed in 1× PBS and biotinylated using an ImmunoProbe Biotinylation Kit (Millipore-Sigma, St. Louis, MO) according to the manufacturer's protocol. The same protocol was used to also biotinylate a matched human IgG_1 myeloma protein (Fitzgerald, Acton, MA). The ability of biotinylated hJAA-F11 H2aL2a to recognize TF-Ag-BSA was confirmed using ELISA probed with streptavidin linked to alkaline phosphatase. Antibody purity was determined using SDS-PAGE to confirm that there was no change in antibody structure such as cross-linking or degradation following modification. Concentrations were determined using A280 absorbance as well as a BioRad protein concentration reagent (BioRad, Hercules, CA).

Radiolabeling of hJAA-F11 H2aL2a via the Bolton-Hunter Method

The indirect radioiodination of the hJAA-F11 H2aL2a antibody was performed using the indirect Bolton-Hunter method as described earlier [13,40,41]. One hundred micrograms of N-succinimidyl-3-(4-hydroxyphenyl propionate) (SHPP) (Thermo Scientific, USA) was added to 2 mg of hJAA-F11 H2aL2a (10 mg/ml in sodium borate buffer) and incubated on ice with mixing once every 30 minutes for 3 hours. Nonreacted SHPP was removed by dialysis against Tris buffer (0.125 M Tris•HCl, pH 6.8, 0.15 M NaCl). The indirect method was utilized to label lysines rather than the direct method which labeled tyrosines and resulted in a loss of reactivity likely due to the number of tyrosines in the CDRs. The product of the reaction was quantitated by BioRad protein assay and analyzed to determine maintenance of *in vitro* antigen binding against TF-Ag-BSA by ELISA [12,13].

Four to seven mCi of ^{124}I in 0.02 M of sodium hydroxide (IBA Molecular North America Inc., VA, USA) was directly added to the precoated iodination tube (Thermo Scientific, USA), and the SHPP linked H2aL2a was mixed with sodium borate buffer (pH 8.5, 100mM) and incubated in the iodination tube at room temperature for 6 minutes. The reaction was stopped by adding 50 μl of scavenging buffer (10 mg tyrosine/ml in Tris iodination buffer). The radiolabeled antibody in the reaction mixture (~2 mg) was isolated using a Dextran Desalting Column (Thermo Scientific, USA) with Tris/NaCl/EDTA buffer as the elution buffer. The activity of each fraction was measured using a Capintec Radioisotope Calibrator, CRC-12. The purity of each fraction was determined by HPLC. The ^{124}I-hJAA-F11 H2aL2a was analyzed for its TF-Ag binding activity by radioimmunoassay to ensure that no loss of reactivity towards the TF-Ag occurred due to radiolabeling [13].

Animals and Tumor Models

Female BALB/c mice (Harlan, Madison, WI), 8 to 10 weeks of age, were used in micro-positron emission tomography (PET) imaging and biodistribution analysis of 4T1 breast tumors. All mice were housed in accordance with the Institutional Animal Care and Use Committees regulations in an Association for Assessment and Accreditation of Laboratory Animal Care International Accredited Facility (University at Buffalo), IACUC#CLS01122Y. All mice were divided into two groups: group I with tumor-bearing mice and group II with non–tumor-bearing mice. 4T1 murine breast cancer cells were implanted by injecting 2.5×10^4 cells in 100 μl of Dulbecco's phosphate-buffered saline subcutaneously under the right nipple while mice were anesthetized with isoflurane/oxygen. Mice were given cold potassium iodide water (0.2 g/l, ad libitum in their drinking water to block thyroid uptake of ^{124}I) and rabbit immunoglobulin (3 mg/mouse, to block Fc receptor uptake) prior to injection of the radiolabeled antibody. Potassium iodide was then given in water for the entire duration of the experiment starting 3 days prior. Mice were administered radiolabeled ^{124}I-hJAA-F11 H2aL2a

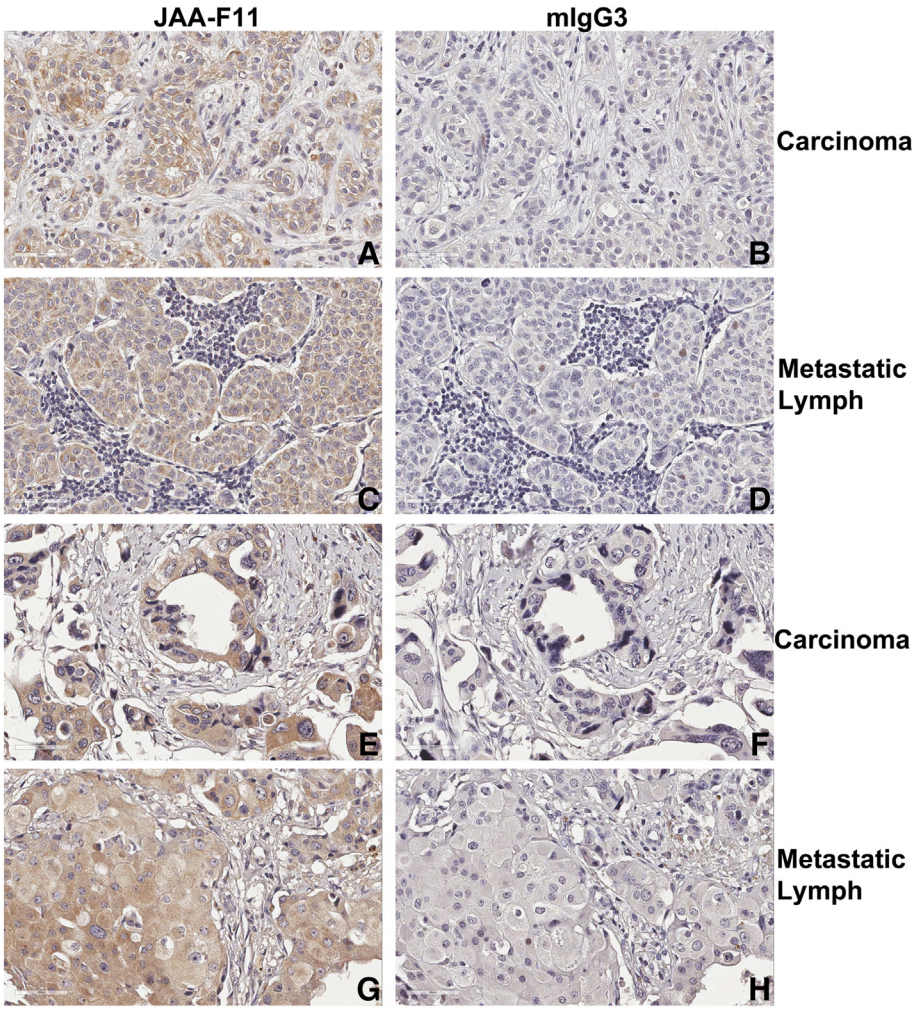

Figure 2. Representative JAA-F11 antibody staining of matched human breast cancer with metastatic lymph nodes. Two representative cases from two patients with invasive ductal breast carcinoma with pathologic diagnosis as documented by US Biomax are shown. Case 1 (A-D) and case 2 (E-H) are shown with JAA-F11 staining specifically (left) compared to matched isotype $mIgG_3$ control (right)**.** Each case was compared for the original breast carcinoma to the metastatic lymph of each patient (A, B to C, D and E, F to G, H). Magnification: 40×.

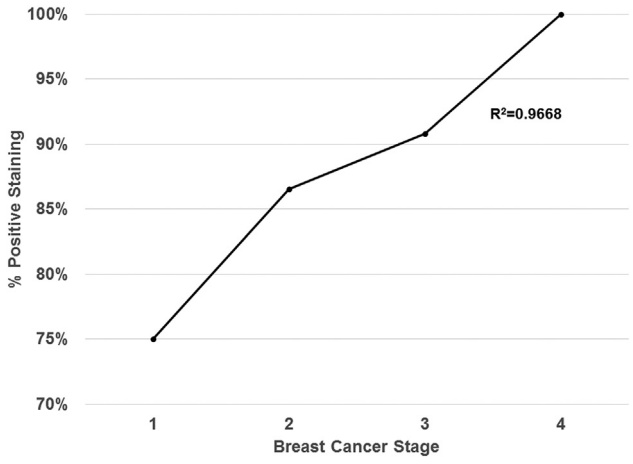

Figure 3. JAA-F11 reactivity with breast cancer by stage. Total JAA-F11 reactivity (percent of cases with positive JAA-F11 staining) plotted relative to increasing breast cancer stage. JAA-F11 reactivity is positively correlated with more advanced breast cancer stage.

(40 μg of antibody in 100 μl of Tris buffer) by tail vein injection at 14 days following tumor cell administration and were analyzed to determine biodistribution and micro-PET imaging. The total administered radioactivity for each individual mouse was determined by measuring the ^{124}I-hJAA-F11 H2aL2a loaded syringes before and after injection with a CRC-12R dose calibrator.

For the human lung tumor xenograft imaging study, human lung cancer cells HTB-171 (NCI-H466, ATCC) were implanted by injecting 8×10^6 cells in 100 μl of DPBS subcutaneously in the left flank of 8- to 10-week-old female nude mice (Jackson Laboratories, Bar Harbor, ME). The remainder of the protocol follows that as described above.

micro-PET Imaging

For whole body imaging of tumor-bearing mice, a Focus 120 micro-PET camera (Siemens Concorde Microsystems previously CTI Concorde Microsystems) was used as previously described [12,13]. The emission scan window was set between 350 and 750 keV. The transmission scan of some mice was also performed using a Cobalt-57 point source for 9 minutes. The transmission scan window was set between 120 and 125 keV. Analysis of the acquired data and image

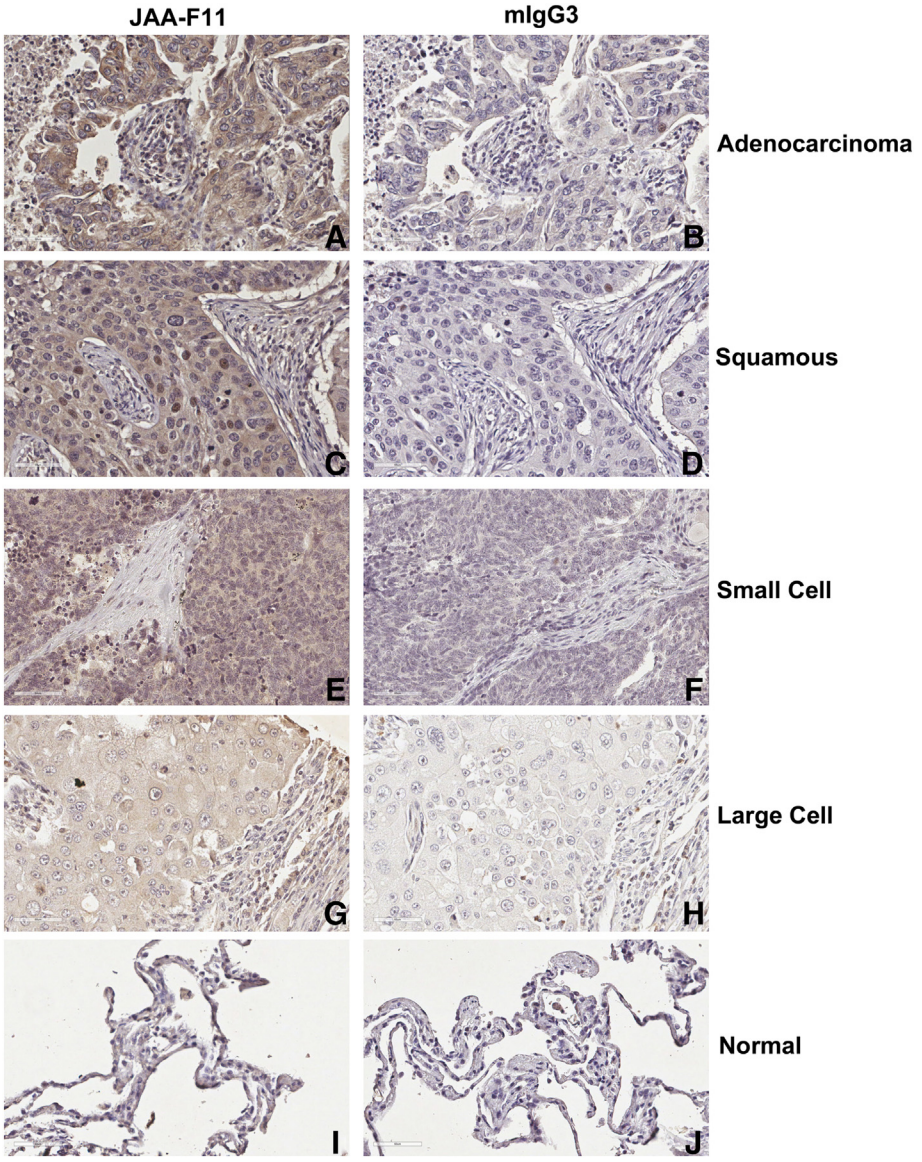

Figure 4. Representative images of human lung cancer staining with JAA-F11 antibody. JAA-F11 staining specificity (left) is compared to matched isotype mouse IgG_3 ($mIgG_3$) control (right). Staining is shown for lung cancers as categorized by US Biomax. The most common lung cancer types were selected: adenocarcinoma (A, B), squamous cell carcinoma (C, D), small cell carcinoma (E, F), and large cell carcinoma (G, H). Staining of normal lung tissue is shown in (I, J). Magnification: 40×.

reconstruction using filtered back projection 2D were done using the software micro-PET manager 2.2.4.0. Before scanning, the mice were anesthetized with oxygen/isoflurane (2% induction, followed by 1% maintenance isoflurane) and placed in the prone position in the gantry of the micro-PET scanner. To analyze and localize the tumor based on metabolic rate, the radiolabeled glucose analog ^{18}F-fluorodeoxyglucose (FDG) was used as a positive control. A 20-minute scan was performed for the ^{18}F-FDG (IBA Molecular North America Inc., VA, USA) images. Three mice with tumors and one without a tumor were selected and imaged 90 minutes after injection of ^{18}F-FDG (10.8-61.2 MBq). One day after FDG imaging, 580.9 to 2501.2 MBq of ^{124}I-hJAA-F11 H2aL2a was injected into 12 mice with tumors and 9 without, and micro-PET imaging was performed at 48, 72, 96, and 168 hours on the mice that had been imaged with the ^{18}F-FDG. The mice were scanned for 30 minutes to obtain images.

Biodistribution and Tumor Uptake Studies

Following imaging at 48, 72, 96, and 168 hours, three mice in each group were sacrificed by injecting 0.1 ml sodium pentobarbital (Fatal Plus) intraperitoneally. Blood, muscle, liver, lungs, kidneys, spleen, heart, stomach, large and small intestines, brain, and tumor tissue were weighed, and the amount of radioactivity was quantified in the gamma-counter with appropriate calibration. Radioactivity uptake was calculated as the percentage of the injected dose per gram of tissue (%ID/g). The total applied radioactivity was determined as above. The percentage of injected dose (%ID) was corrected for decay utilizing two accompanying standards at the time of each biodistribution.

Results

Our previous studies of JAA-F11 were carried out in a murine breast tumor model to confirm the feasibility JAA-F11 as a breast cancer

Table 3. Positive Staining of Specific Lung Cancer Cases with JAA-F11

(A)

JAA-F11 Reactivity by Lung Cancer Type

Pathology	# Positive	# Of Cases	% Positive
Adenocarcinoma	52	75	69%
Large cell carcinoma	13	16	81%
Squamous cell carcinoma	50	52	96%
Small cell carcinoma	37	38	97%

(B)

JAA-F11 Reactivity of Malignant Lung Cancer By Gender

Sex	# Positive	# Of Cases	% Positive
Male	132	155	85%
Female	41	48	85%

(C)

JAA-F11 Reactivity of Lung Tumors and Matching Lymph Nodes

Type	# Positive	# Of Cases	% Positive
Tumors	20	28	71%
Lymph nodes	22	28	79%

(A) Percentages of TF-Ag–Positive Staining Lung Cancers Broken Down by Lung Cancer Cell Types. (B) JAA-F11 Staining of Lung Cancer Cases According to Known Genders. (C) Staining of Lung Cancer Tumors in Patients That Also Had Metastasis to Lymph Nodes.

therapy. JAA-F11 binds the murine breast cancer cell line 4T1 and human breast cancer cell lines; increases mice survival; and prevents metastasis of breast, prostate, and colon cancer cells through binding of TF-Ag *in vivo* and *in vitro* [12,17,18,42–45]. Other studies have suggested that TF-Ag could be present on up to 80%-90% of human cancers [22,46–50]. To comprehensively assess the potential of JAA-F11 to selectively target a wide range of different human cancer types, the present study used IHC to screen an extensive panel of human tumor and normal tissues.

Human cancer tissue microarrays were obtained from US Biomax (Rockville, MD) and evaluated using a paired murine IgG_3 negative control microarray slide in IHC. Several cancer types were selected, including cancers of breast, lung, ovary, colon, prostate, and bladder. Positive tissue reactivity with JAA-F11 was found for 85% of all individual carcinoma cases tested (n = 1269) after subtracting the nonspecific staining score with the IgG_3 control from the JAA-F11 score. Breast, prostate, and bladder cancer cases were ~90% reactive with JAA-F11, while lung, colon, and ovarian cancer cases were ~80% to 85% reactive with JAA-F11 (Table 1). The high amount of positive IHC staining with all tested carcinoma cases demonstrates the prevalence of JAA-F11 binding TF-Ag on a wide array of human cancer cells.

For breast cancer cases, the expression of the estrogen receptor (ER), progesterone receptor (PR), and/or the human epidermal growth factor receptor 2 (HER2) makes these tumors receptive to common targeted therapies available today. However, tumors with the absence of the expression of these receptors, triple-negative breast cancer or TNBC, represent the most aggressive and hardest to specifically treat breast cancers, which rely largely on chemotherapy regimens. Breast cancer microarray slides with all types of breast cancers were screened using IHC with JAA-F11 and a matched mouse isotype IgG_3 control (Figure 1, Table 2*A*). JAA-F11 strongly stained all types of breast cancer, including TNBC (Figure 1, *A-B*). Representative normal breast tissue without staining reactivity is also shown (Figure 1, *I-J*). Table 2*A* summarizes the human breast cancer array data by cancer subtype, including TNBC (ER–/PR–/HER2–), ER+/PR+, ER+/PR–, PR+/ER–, and HER2+ cases. JAA-F11 was extremely effective at binding to all of these breast cancer subtypes, including 94% of the 126 cases of TNBC, a tumor type that currently has no targeted therapy. Breast tumor types that were underrepresented are not shown in the table [e.g., ER+, PR+, and HER2+ (known as triple positive) were less than 3% of specimens]. Some of the breast cancer cases were not stratified by receptor status; therefore, the exact percentage positive shown varies slightly from Tables 1 to 2*A*.

Breast tumor staging information was also provided in the majority of the cancer tissue arrays. Stratifying by cancer stage, the summary data in Table 2*B* show that stage I breast cancer cases were 75% positive, stage II 87%, stage III 91% and that 100% of the stage IV samples reacted with JAA-F11 antibody, showing a positive correlation with metastatic tendency (Table 2*B* and Figure 2). Some of the tissue arrays also contained patient matched lymph node metastases (Figure 3 and Table 2*C*), where reactivity to primary tumors and the metastases was consistently similar. This indicates that both the original tumor and its metastatic site tumor retained TF-Ag expression.

The most common cause of cancer-related death is lung cancer; therefore, the ability of JAA-F11 to bind lung cancer types was also a focus of this IHC analysis. The lung tumor reactivity data were stratified by cancer type into the major groups of small cell lung cancers (SCLCs) and the non–small cell lung cancers (NSCLCs), which include adenocarcinomas, squamous cell carcinomas, and large cell carcinomas (Figure 4 and Table 3*A*). Of the NSCLCs, squamous cell carcinomas had the highest percentage of TF-Ag reactive samples with 96% of the 52 samples being positive. Sixty-nine percent of the 75 cases of NSCLC adenocarcinomas were reactive. The NSCLCs categorized as large cell carcinomas showed consistent TF-Ag reactivity, with an 81% positivity rate for the 16 tumors that were tested, but displayed an overall lighter staining than other lung cancers. Ninety-seven percent of the 38 cases of SCLCs were positive. Concerning analysis of gender differences, the proportion of tumor tissues in the tested tissue microarrays with male compared to female cases was slightly higher than the natural lung cancer prevalence according to the CDC. Our sample consisted of 76.3 % men, while men with lung cancer will account for 52.6 % of all lung cancer cases [51]. Table 3*B*, stratified by gender, shows similar TF-Ag reactivity (both 85%) in male and female cases of lung cancer. Some of the slides also contained matching lymph node metastases (Table 3c), in which the binding of JAA-F11 to primary tumors and the matched metastases was similar. This is in agreement with the breast cancer metastatic lymph node data (Figure 2*C*) and confirms that the TF-Ag expression in lung cancer was retained following tumor metastasis.

Ovarian cancer represents one of the highest mortality rates of female cancer types, having a less than 50% survival rate within 5 years of diagnosis, making it a good candidate for new targeted therapies. Various types of ovarian cancers from 390 cases were analyzed using JAA-F11. Similar to other types of cancers that were tested, JAA-F11 was able to specifically stain 81% of cancer cases of ovarian origin (Table 1). These included many cases of adenocarcinomas (Figure 5), as well as other tumor types such as yolk sac tumors and teratomas, with little staining on normal ovary cells.

Other carcinoma types were also analyzed using JAA-F11, including bladder, colon, and prostate. After breast and lung cancers, prostate and

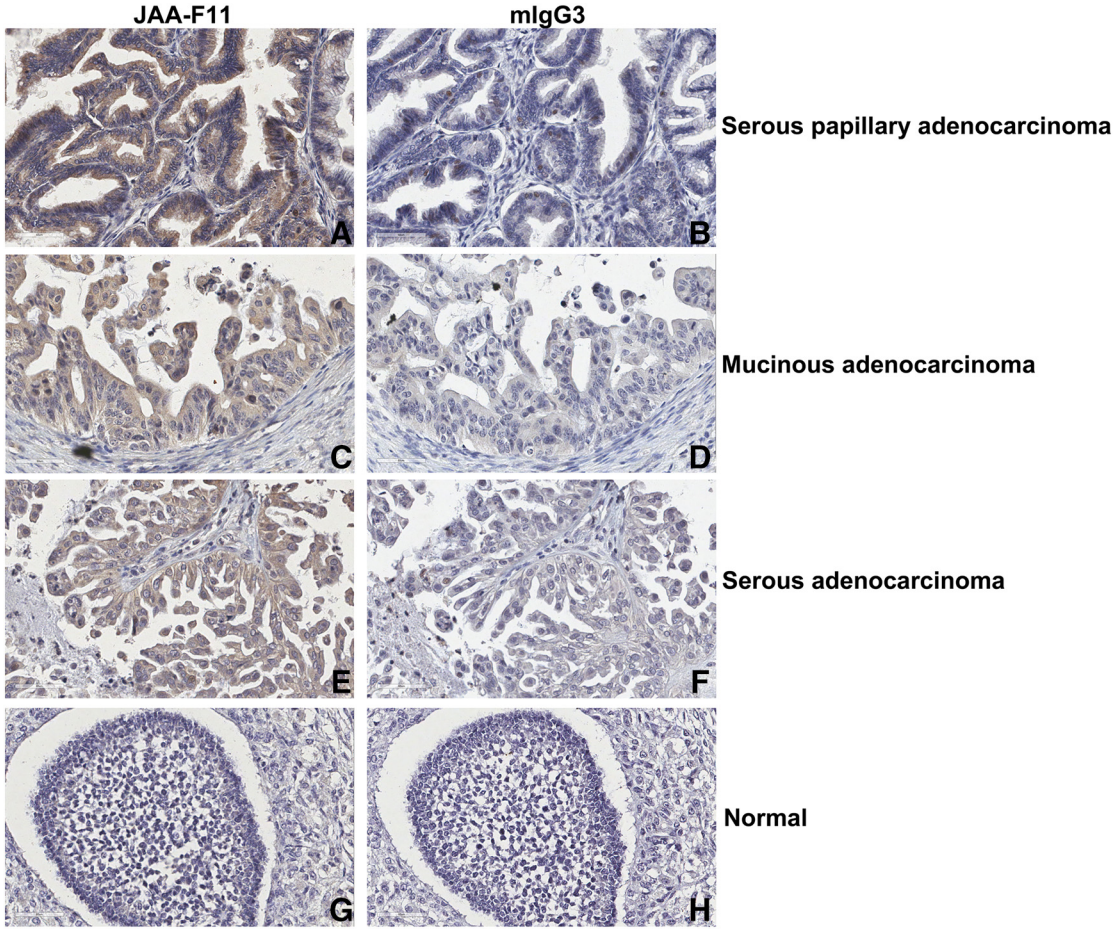

Figure 5. Representative images of human ovarian cancer staining with JAA-F11 antibody. Staining with JAA-F11 and matched isotype mouse IgG_3 ($mIgG_3$) control was performed on cancer and normal tissue for various ovarian cancer types (A-F) and for normal ovarian tissue (G, H). Magnification: 40×.

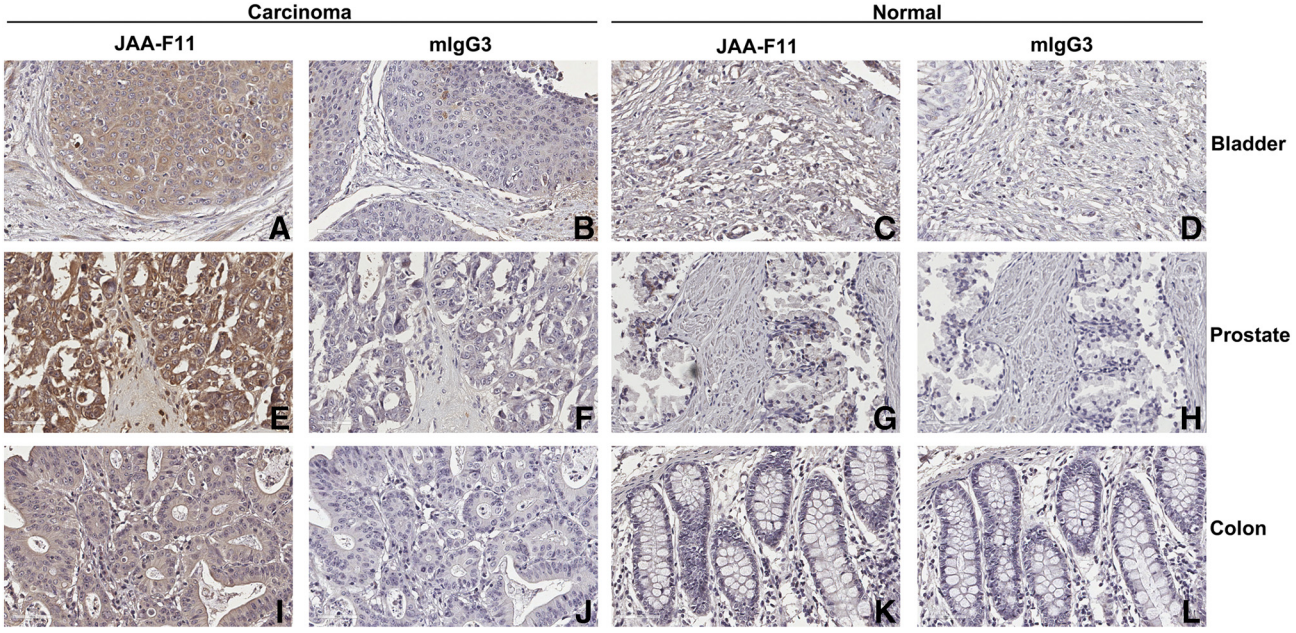

Figure 6. Representative images of human colon, prostate, and bladder cancer staining with JAA-F11 antibody. Staining with JAA-F11 and matched isotype mouse IgG_3 ($mIgG_3$) control was performed on cancer and normal tissue for bladder [cancer (A, B) and normal (C, D)], prostate [cancer (E, F) and normal (G, H)] and colon [cancer (I, J) and normal (K, L)]. Magnification: 40×.

Table 4. Staining of Normal Human Tissues by JAA-F11 and Effect of Preincubation with TF-Ag-BSA

(A)

Normal Tissue Showing No Staining Using JAA-F11

Tissue	% Reactive
Bronchus	0% (0/1)
Diaphragm	0% (0/1)
Eye	0% (0/3)
Intestine	0% (0/2)
Lymph	0% (0/5)
Nerve	0% (0/2)
Parathyroid	0% (0/2)
Salivary	0% (0/2)
Thymus	0% (0/5)
Thyroid	0% (0/7)

(B)

Normal Tissue With Nonspecific Staining Using JAA-F11

Tissue	% Reactive	Inhibitable With TF-Ag
Adrenal	88% (7/8)	-
Bladder	25% (2/8)	-
Bone	38% (3/8)	-
Breast	19% (5/26)	-
Cerebellum	43% (3/7)	-
Cerebrum	21% (4/19)	-
Colon	41% (7/17)	-
Esophagus	88% (7/8)	-
Heart	29% (2/7)	-
Hypophysis	38% (3/8)	-
Kidney	25% (2/8)	-
Larynx	25% (1/4)	-
Lung	10% (10/98)	-
Ovary	16% (6/38)	-
Prostate	50% (13/26)	-
Skeletal Muscle	25% (1/4)	-
Skin	71% (5/7)	-
Spleen	22% (2/9)	-
Testis	80% (4/5)	-
Tongue	33% (1/3)	-
Tonsil	50% (4/8)	-
Uterus	25% (2/8)	-

Table 4c

Normal Tissue With Inhibitable Staining Using JAA-F11

Tissue	% Reactive	Inhibitable With TF-Ag*
Pancreas	63% (5/8)	+
Stomach	57% (4/7)	+
Liver	44% (4/9)	+

(A) Normal human tissue types that did not display staining in the presence of mJAA-F11 based on all data presented in Supplemental File 1. (B) Normal human tissue samples that displayed some degree of nonspecific staining with JAA-F11. Percentages are based on total positive samples from Supplemental File 1. Each tissue was observed in experiments involving preincubation with TF-Ag-BSA detailed in Supplemental File 3, and no inhibition of staining was observed, indicating that staining seen was nonspecific. (C) Normal human tissue samples that displayed some specific inhibition of JAA-F11 staining using soluble TF-Ag-BSA. The total reactive tissues are derived from multiple samples from Supplemental File 1. Each tissue was observed in experiments involving preincubation with TF-Ag-BSA on the same slides as those tissues in B. Specific inhibition percentages are displayed in Footnotes. All of the pancreas samples showed inhibition of staining, indicating that specific staining was seen in all samples. With stomach and liver, only some of the samples showed specific inhibition of staining.

colorectal cancers are the third and fourth most common cancers in the United States, according to the NCI (https://www.cancer.gov/types/common-cancers). As seen with breast and lung cancers, JAA-F11 showed a distinct, selective staining on cancer cells from 90% of the cases of bladder, 80% of colon, and 93% of prostate cancer cases (Table 1 and Figure 6), with little to no staining on surrounding normal tissue.

As any therapeutic treatment that relies on the specific targeting of the antibody to only cancer cells and not to normal tissues, the ability of mouse JAA-F11 to not bind to and stain normal human tissue arrays was extensively investigated. It should be noted that the normal tissue arrays that were obtained consisted of cadaver-derived tissue rather than the normal adjacent tissue that accompanied the cancer arrays detailed above which are rapidly fixed after surgical resection. The cadaver normal tissue harvesting can begin up to 6 hours after death and take an additional 6 hours before harvesting is complete. Additionally, the appearance of some of the normal tissue on these slides showed some changes consistent with autolysis including degraded-looking tissue and pale or absent nucleus in the cells. Therefore, we considered the possibility of alterations occurring in these normal tissues. In a total of 35 different normal tissue tested, no staining was observed in 9 tissue types (Table 4*A*), 22 tissue types showed light staining (Table 4*B*) that was weaker than the staining observed in tumor (Figure 7, *A-X*), and 4 tissues showed strong staining and these included the esophagus (on Table 4*B*), pancreas, stomach, and liver (Table 4*C*). Normal tissue arrays which had better tissue integrity showed consistently lower overall background staining and in the majority of cases presented no staining. Staining, when detected, was noted in areas such as stratified squamous epithelia (e.g., esophagus), glandular structures and/or secretions (e.g., adrenal gland, pancreas, stomach), testis, and pancreatic islet cells, as well as light staining in areas that would not be therapeutically accessible (e.g., cerebrum) (Table 4). To determine whether this was specific or nonspecific reactivity of the normal tissue, a preincubation of the antibody preparation with TF-Ag-BSA to remove the specific JAA-F11 antibody reactivity was performed, and this preparation was used on both tumor and normal tissue arrays. To determine the efficacy of this preincubation, the pretreated antibody was tested on arrays containing tumor sections. Prior to addition of JAA-F11 to a prostate tumor array, JAA-F11 was preincubated with either IHC grade BSA or TF-Ag-α linked to BSA. TF-Ag-BSA is routinely utilized as a coating antigen to test JAA-F11 via ELISA assays [17,52]. In this situation, JAA-F11 is blocked by the added TF-Ag and expected to be unable to bind TF-Ag presented on the tumor arrays. Remaining staining following preincubation with TF-Ag-BSA was considered to be nonspecific. Testing through ELISA confirmed that binding to plate-bound TF-Ag-BSA was reduced 75% when JAA-F11 was preincubated with TF-Ag-BSA in solution (data not shown). When JAA-F11 was preincubated with BSA only, ELISA reactivity remained, and strong staining of prostate tumor cells was observed, while preincubation with TF-Ag-BSA at the same concentration greatly diminished tumor staining, confirming the efficacy of the preincubation and the specific reactivity of JAA-F11 with TF-Ag on tumor tissues (comparison shown in Figure 8). For the prostate cancer array subjected to TF-Ag-BSA preabsorption, the amount of positive staining prostate cancer samples that were inhibited was 98% (58/59 positive cases; Supplemental File 3). When this TF-Ag preincubated JAA-F11 was utilized on a normal autopsy tissue array, JAA-F11 staining was reduced only in the pancreatic islet cells (100% of samples), stomach gastric cells (50% of samples), and hepatic cells (25% of samples)(Figure 9 and Table 4*C*), suggesting that the staining on cells of these normal tissues is specific in these cases, whereas the observed staining in all the other normal tissue types (where staining was not reduced) is nonspecific (Figure 10 and Table 4*B*). Further

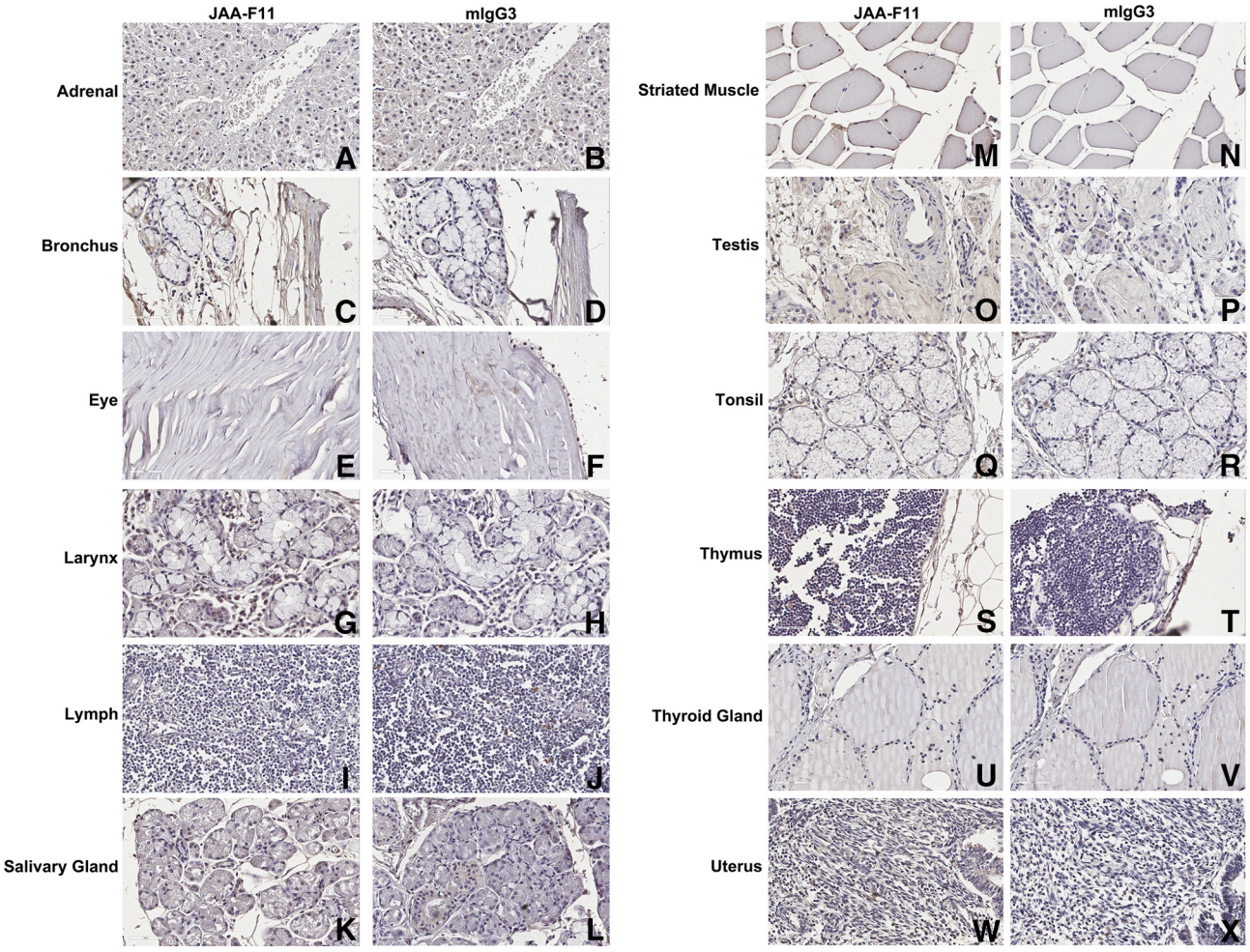

Figure 7. Representative images showing little to no staining on human normal tissues with JAA-F11 antibody. Staining with JAA-F11 and matched isotype mouse IgG_3 ($mIgG_3$) control was performed on multiple normal human tissues (A-X). Magnification: 40×.

experiments using preincubations were also performed using a general cancer array and two more normal human tissue arrays to fully determine the extent and specificity of mouse JAA-F11 staining *in vitro*. The cancer array showed the same trend that was seen in the prostate cancer array, with 73% of carcinomas showing TF-Ag–dependent specific inhibition following preincubation with soluble TF-Ag-BSA (Supplemental File 3). This array also displayed inhibition of other cancers outside of the scope of this study including thyroid, pancreas, and testis. The normal tissue arrays done in parallel showed almost no inhibition of staining following preincubation, again showing that the observed IHC staining of most normal tissue is nonspecific. In one of these additional arrays, one specimen (n=1) of fallopian tube, a previously untested tissue, was tested and the light staining it exhibited was inhibitable. This inhibition will be investigated in future studies due to its low sample number in this study (Supplemental File 3).

To determine if IHC staining would be improved by investigating the staining potential using the recently characterized hJAA-F11 H2aL2a [52], an IHC assay was designed using biotinylated hJAA-F11 to circumvent problems using a secondary labeled anti-human immunoglobulin on human tissue. Using a biotinylated human myeloma IgG1 protein as a matched control, the staining of biotinylated hJAA-F11 H2aL2a was assessed against a human breast cancer array and a normal human tissue array. This staining was also compared against that of normal human tissue staining using the mouse JAA-F11 done in parallel. Like the original mouse antibody (Figure 1), biotinylated hJAA-F11 H2aL2a was able to specifically stain human cancer cells in the breast cancer array, including cases that were ER+/PR+ and TNBC, while there was little to no staining with the biotinylated human IgG_1 (Figure 11, *A-D*). Importantly, several normal human tissues which had shown high backgrounds with the mouse antibody including esophagus and kidney (Figure 10) showed markedly lower background staining using the biotinylated human antibody, while retaining the ability to stain the breast cancer cells (Figure 11). As the humanization of JAA-F11 is required for therapy with JAA-F11, these data confirm the potential of hJAA-F11 H2aL2a seen *in vivo* efficacy studies [37].

To evaluate the biodistribution properties of hJAA-F11 H2aL2a, TF-Ag–positive 4T1 murine breast tumors were established in female Balb/C mice as described earlier [17]. Biodistribution analysis was performed in tumor-bearing (n=12) and non–tumor-bearing (n=9) mice. One day before the ^{124}I-hJAA-F11 H2aL2a injection, the metabolic marker ^{18}F-FDG was administered for positive control for tumor localization. In tumor-bearing mice, localization of ^{18}F-FDG was observed in high metabolic areas including tumor with high uptake as shown in Figure 12*A*. In the non–tumor-bearing mice, ^{18}F-FDG uptake was seen in only high metabolic areas (data not shown).

Three tumor-bearing mice and one non–tumor-bearing mouse were imaged at 48, 72, 96, 144, and 168 hours after ^{124}I-hJAA-F11 H2aL2a injection. The specificity of binding to TF-Ag on tumor cells was

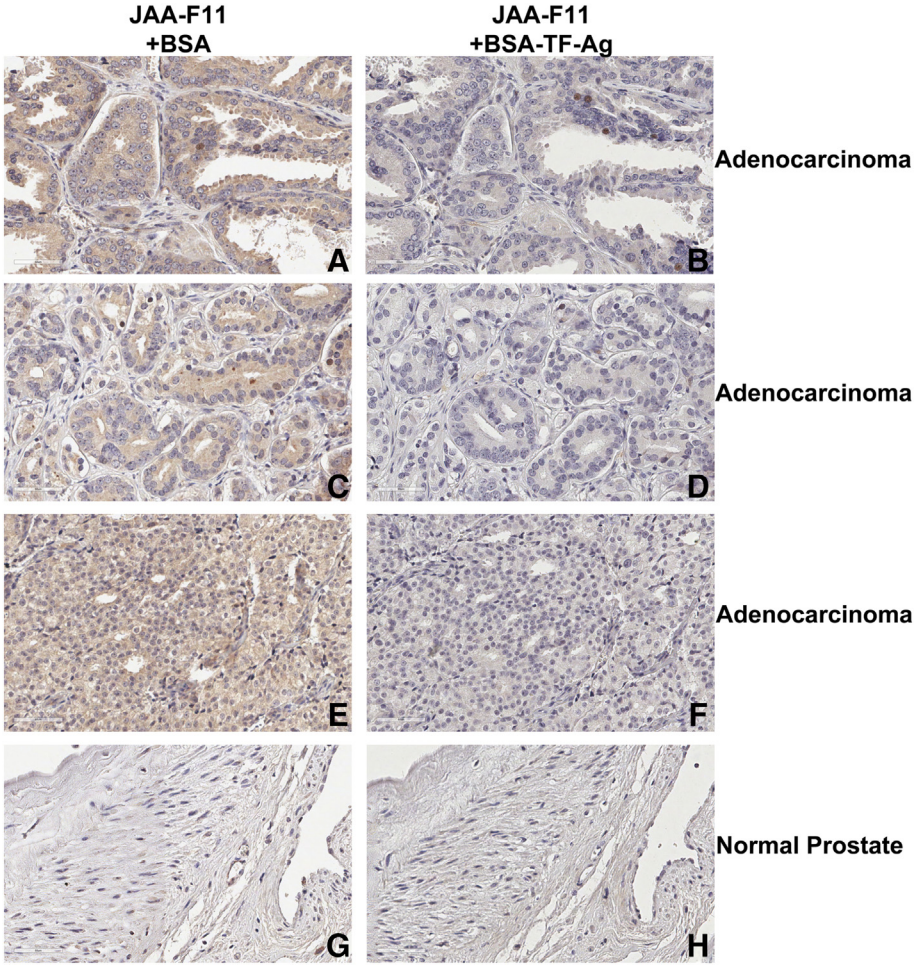

Figure 8. Representative images of JAA-F11 antibody staining on human prostate cancer tissue with or without preabsorption with TF-antigen. Three cases of human prostate cancer are shown (A-F) with JAA-F11 staining without TF-antigen (only BSA) (left) or with preincubation with TF-antigen (TF-Ag-BSA) (right). Images (A-F) confirm specific TF-Ag staining on prostate cancer. Images (I, J) show no staining on normal prostate tissue. Magnification: 40×.

evidenced by the observed high uptake of ^{124}I-hJAA-F11 H2aL2a in the tumor of the 4T1 tumor-bearing mice and lack of reactivity in the non–tumor-bearing mouse (Figure 12, *C* versus *D*). At 48 hours, high background signal from normal tissues such as heart and lungs was observed along with specific imaging of the tumor due to the presence of labeled antibody in the blood. However, at this time point, ^{124}I-hJAA-F11 H2aL2a uptake in the tumor was significantly higher than background, allowing clear imaging of the tumor (Figure 12*C*). By 72 hours, average tumor uptake of ^{124}I-hJAA-F11 H2aL2a determined by tissue distribution was 5.0±1.36%ID/g and represented the highest amount of radiolabel of all analyzed tissues with the exception of blood (Figure 13). Uptake of ^{124}I- hJAA-F11 H2aL2a increased slightly to about ~5.7% ID/g, which persisted to the last imaging time point taken at 7 days postinjection. Average uptake of the ^{124}I-hJAA-F11 H2aL2a in the heart, liver, and muscle decreased to 0.05, 0.5, and 0.2%ID/g respectively at 168 hours (Figure 13 and Supplemental Table 1). Note that the high blood levels in the early time points in Figure 13 result in the heart and lung hot spots in the early time points in the imaging (Figure 12). This is consistent with the biodistribution results seen by others with radiolabeled whole antibody [53–55]. Note that all tissues except tumor and kidney have parallel decreasing lines in Figure 13, indicating that no specific tissue accumulation is occurring. Kidney transiently increases slightly due to the fact that it is a clearing site of free ^{124}I, while the amount in the tumor as a % of injected dose increases at each time point (Figure 13). ^{124}I-hJAA-F11 H2aL2a in the non–tumor-bearing mice did not show significant or specific uptake. By 144 hours, no radiolabeled signal was observed in control mice as shown in the Figure 12*D* control panel. Importantly, these *in vivo* organ imaging and biodistribution studies with ^{124}I- hJAA-F11 H2aL2a at 7 days support the IHC findings that the hJAA-F11 H2aL2a has negligible binding to normal tissues.

To further expand the applicability of hJAA-F11 H2aL2a in an *in vivo* model, HTB-171 (NCI-H446) human lung cancer cells were injected into female nude mice in a study consisting of only PET imaging. Once tumors were palpable on day 18 postinjection, ^{124}I-hJAA-F11 H2aL2a was injected into mice, and localization was tracked as in the prior experiment. As with the breast cancer murine model, ^{124}I-hJAA-F11 H2aL2a was found to specifically target the lung tumor in the nude mouse model and persist in the tumor for at least 7 days (Figure 12*D*). In conclusion, our results showed that ^{124}I-hJAA-F11 H2aL2a antibody is a superior *in vivo* imaging agent because of low nonspecific uptake and specific tumor-to-soft tissue contrast.

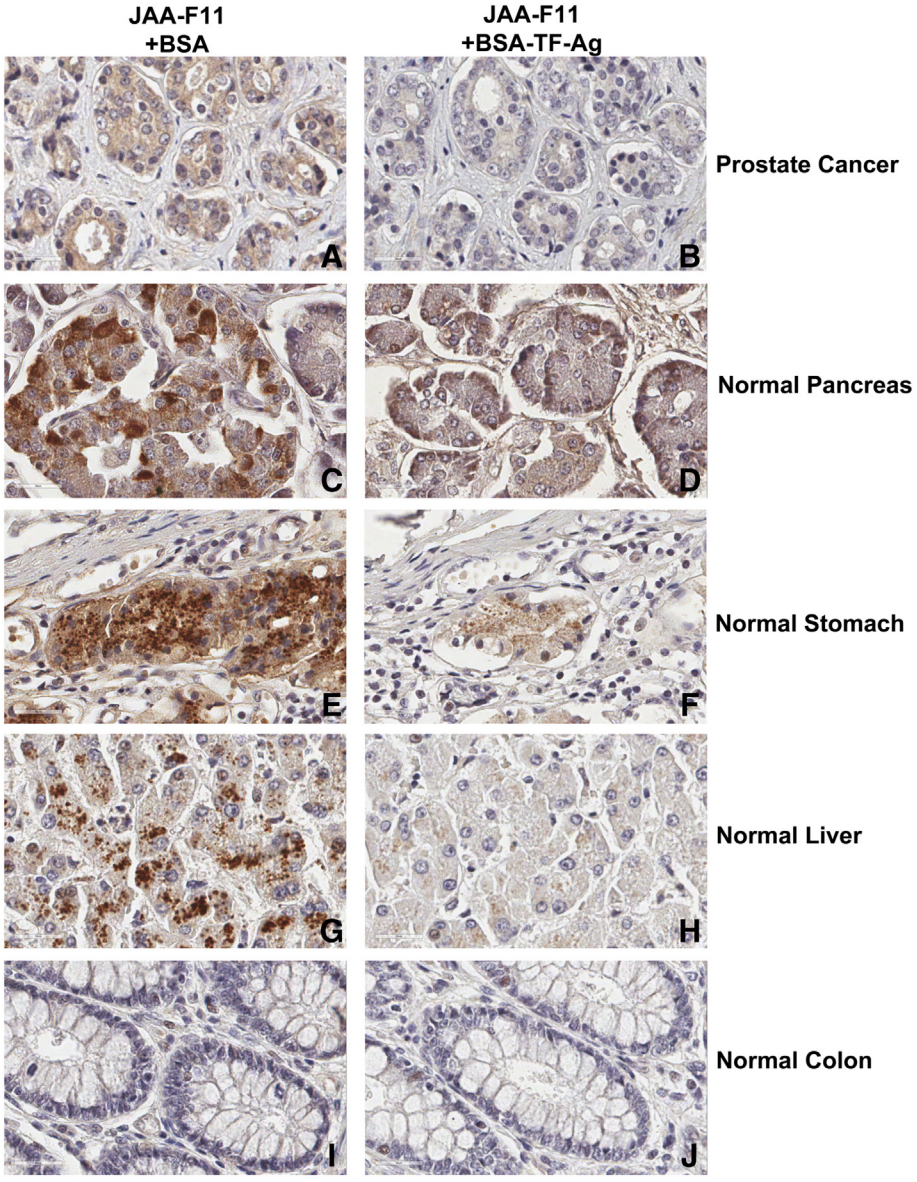

Figure 9. Images of JAA-F11 antibody staining on normal human tissue with or without preincubation with TF-antigen. A representative prostate cancer case (A-B) and four types of human normal tissue are shown (C-J) with JAA-F11 staining without TF-antigen (only BSA) (left) or with preincubation with TF-Ag-BSA (right). Images A and B confirm specificity of TF-Ag staining on prostate cancer, similar to that shown in Figure 8. Specific, inhibitable staining of specific cells was seen in only normal pancreas, stomach, and liver tissue since the TF–Ag positive cells were decreased upon preincubation with TF-Ag-BSA (D, F, H). Conversely, colon cells do not show any significant staining with JAA-F11 either in the presence or absence or free TF-Ag (I, J). Magnification: 80×.

Discussion

Targeted therapies for cancers are becoming an increasingly important facet of anticancer strategies. As such, there is a great unmet need for a generalized pancarcinoma marker that can be the basis of such a strategy. Antibody-based therapies such as trastuzumab (breast cancer) and necitumumab (squamous non–small cell lung carcinoma) have shown the power of such avenues but are limited to cancer cell surface markers (HER2/neu and EGF receptor, respectively) that are not overexpressed in the majority of cases. Here the specificity of the anti-TF-Ag antibody JAA-F11 and its humanized derivative hJAA-F11 H2aL2a is described in detail, documenting their specific abilities to selectively bind human tumor cells of many types including breast, prostate, lung, colon, bladder, and ovarian cancers.

Since the initial discovery of the tumor association of TF-Ag over 40 years ago, many studies have attempted to use the tumor cell specific exposure of the core antigen for production of antibodies capable of detecting TF-Ag [30,31,33,56]. However, the consistent problem with these attempts has been the lower specificity of these strategies; wherein the beta linked version of TF-Ag is recognized along with the alpha linked anomer, as well as other elongated or branched carbohydrates found on normal tissues. Additionally, promising antibodies against TF-Ag, such as HH8 [31] and A78-G/A7 [30], are of the mouse IgM isotype, further limiting the potential for theranostic approaches.

The best known earlier anti-TF strategy that made it to Phase III studies is the anti-TF mAb 170H.82 (known as the trademark Tru-Scint). This antibody was withdrawn during human trials, likely due to

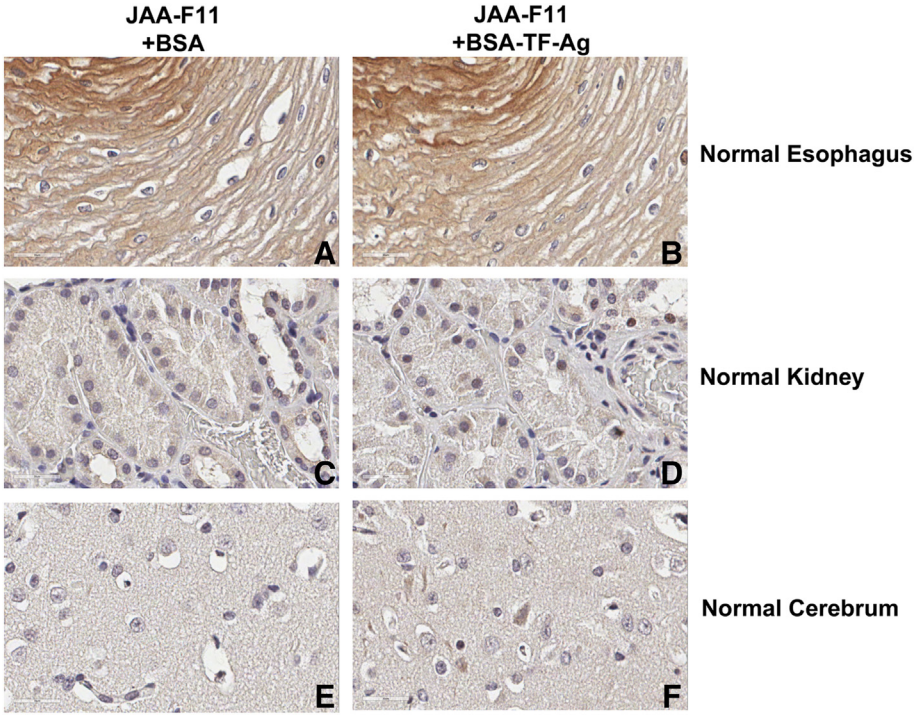

Figure 10. Images of JAA-F11 antibody staining on normal human tissue with or without preincubation with TF-Ag-BSA. Several representative images are shown for tissue types that have a propensity to display background staining with JAA-F11, either with or without TF-Ag preincubation. Three types of human normal tissue are shown (A-F) with JAA-F11 staining without TF-antigen (only BSA) (left) or with JAA-F11 preincubation with TF-antigen (TF-Ag-BSA) (right). These tissue types show a similar degree of staining either in the presence or absence or free TF-Ag (B, D, F), suggesting that these normal tissues show nonspecific staining. Magnification: 80×.

its nonselective binding to both TF-Ag-α and TF-Ag-β structures resulting in off-target binding and accumulation in the kidney or liver [57,58]. Radiolabeled PNA with its binding to both TF-Ag anomers and resultant lack of specificity also showed kidney binding on imaging [59].

Here, we extensively documented the ability of the original mouse JAA-F11 to specifically bind to and stain 85% of tumor tissue from 1269 cases of various types of human cancers, while on the analysis of 35 normal human tissues, 32 of these tissues did not show specific staining. Specific staining was found only on pancreatic islet cells, stomach gastric cells, and hepatic cells (Table 4). It is our hypothesis that staining of these tissues with high enzymatic activity was an artifact of the use of partially autolyzed normal tissues from cadavers. It was reported by Philipsen et al. [60] that cell membrane TF-Ag was absent in 15 of the 15 human pancreas samples that they obtained surgically and immediately fixed. However, they also showed that upon neuraminidase treatment, TF-Ag was revealed after exposure by treatment with *Clostridium perfringens* type X neuramindase in all samples [60]. *Clostridium perfringens* neuraminidase cleaves α 2-3, α 2-6, and α 2-8 linked sialic acid. The normal pancreata used in the IHC in this study, unlike those in the Philipsen study, were obtained at autopsy which began up to a period of up to 6 hours postmortem and took up to 6 hours [38], leaving significant time for autolysis (up to 12 hours). The pancreas is one of the first organs to undergo autolysis, with autolysis of this organ occurring within hours after death [61]. Supporting our hypothesis is the fact that the pancreas is highest in expression of Neu1, a neuraminidase that cleaves both α 2-3 and α 2-6 linked sialic acids [62]. Thus, the Philipsen reports of neuraminidase [60] exposing TF-Ag in normal pancreas and the Monti review [63] describing the high Neu1 expression in the pancreas support our hypothesis that TF-Ag could become exposed on these tissues. Similar theories could be developed for the staining of the normal human liver and stomach samples since these are both organs with enzymatic activity and are among tissues prone to early autolysis [61,64–66]. In addition, liver has a high expression level of biotin, which is commonly problematic in the ABC staining techniques such as utilized here [67], and hepatocytes have high expression of asialoglycophorin receptors [68], which may have bound TF-Ag present. In contrast to normal tissues, tumor tissue has been obtained at surgery and is rapidly fixed and thus would not be expected to show autolytic changes. The mouse liver and the stomach do not have increased levels of ^{124}I JAA-F11 in our imaging and biodistribution studies (Figures 12 and 13), substantiating this hypothesis; however, the pancreas had not been collected in this or any of our previous biodistribution studies. Overall, although suggestive, since our studies cannot conclusively state that there is no possibility of specific binding occurring with the pancreas, stomach, and liver, these organs should be carefully assessed in animal safety analysis and in subsequent Phase I clinical trials.

The recently developed and characterized humanized IgG_1 form of JAA-F11, hJAA-F11 H2aL2a [52], was biotinylated and displayed the ability to specifically stain human breast cancer while also having a lower general nonspecific background on normal tissue compared to the mouse antibody. These results confirm the findings of our inhibition analysis, suggesting that some specific staining was present only on these autopsy specimens of human pancreas, stomach, and liver.

hJAA-F11 H2aL2a and other humanized constructs, which are humanized IgG_1 molecules, are designed for immunotherapy and

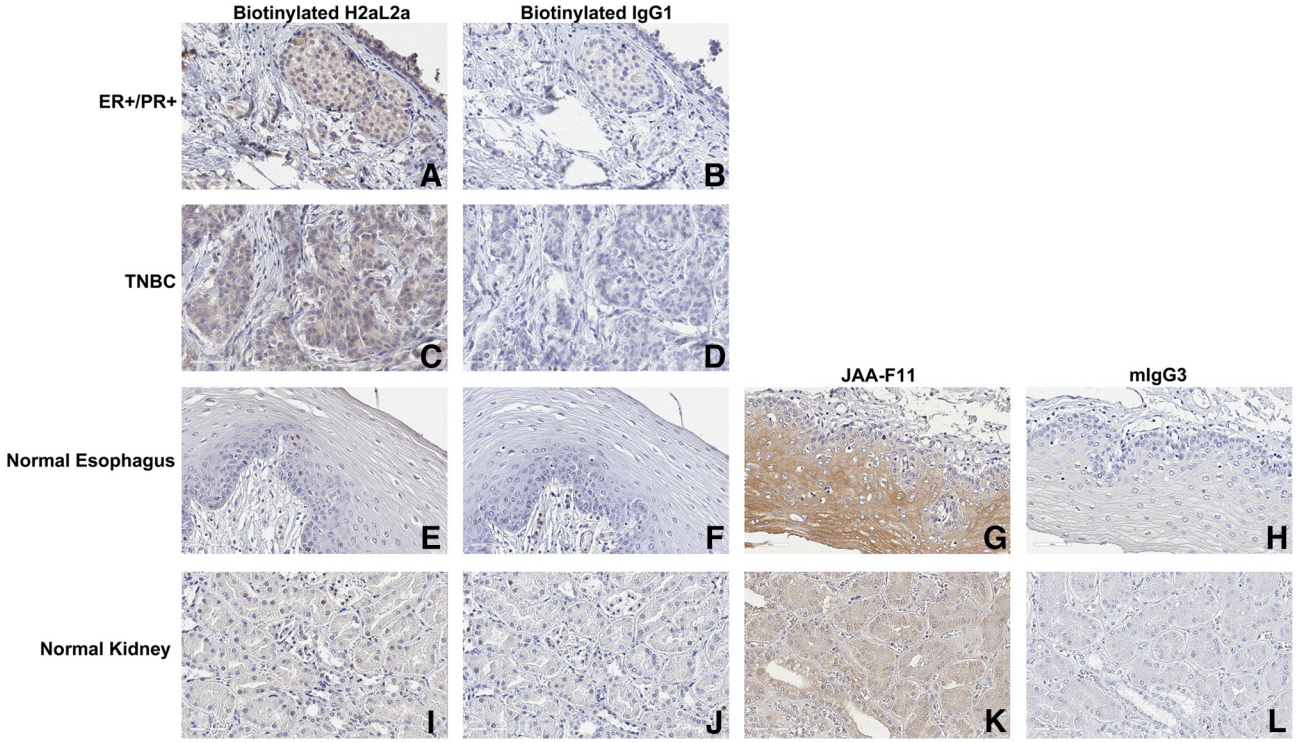

Figure 11. Biotinylated hJAA-F11 H2aL2a exhibits specific staining on human breast cancer but not normal esophagus or kidney. Human breast cancer cases of ER+/PR+ (A-B) and triple negative (TNBC, C-D) were stained using biotinylated hJAA-F11 H2aL2a (A, C) or a biotinylated human myeloma IgG protein (B, D). The background staining differences were also assessed in normal esophagus (E-H) and kidney (I-L) using the biotinylated human antibodies (E-F, I-J) and the mouse JAA-F11 and control mouse IgG_3 antibodies (G-H, K-L). These images indicate that hJAA-11 H2aL2a does not bind to normal human esophagus or kidney. Experiments were done in parallel, and color development was identical for all slides. Magnification: 40×.

theranostics and maintain the same chemical and biological specificity as mouse JAA-F11. Glycan array analysis has documented the highly selective chemical specificity of JAA-F11 and its humanized derivatives for the tumor-associated TF-Ag-α [52,69]. The high specificity of JAA-F11 for TF-Ag-α is due to its ability to recognize TF-Ag through cavity-type glycan binding rather than the more one-sided groove-type antigen recognition. Computational analysis of JAA-F11 revealed that the amino acid composition of JAA-F11's light chain variable region does not allow for the binding to the TF-Ag-β structure while allowing the specific binding to the tumor-associated TF-Ag-α presentation [69]. Therefore, JAA-F11 represents a strong and specific tool for the immunohistochemistry-based assessment of TF-Ag–bearing human carcinomas and future cancer therapeutic applications. Importantly, the IHC and *in vivo* biodistribution and imaging studies also document the tumor-specific binding of hJAA-F11 H2aL2a, with limited or no binding to normal tissues, supporting its preclinical development for cancer immunotherapeutic applications.

Imaging and biodistribution results with radiolabeled hJAA-F11 H2aL2a in the mouse tumor models for both breast and lung cancers also support the specificity of humanized JAA-F11 *in vivo*. While the mouse JAA-F11 did have some IHC reactivity that may be specific against some normal tissue sections from stomach and pancreas, this staining may be due to enzymatically degraded postmortem tissue, and this is supported by the lack of accumulation in stomach and liver in the biodistribution analysis. Furthermore, the differences in tumor retention of the labeled antibody compared to the time course of retention in all other organs confirm that humanized JAA-F11 was not retained in any normal organ examined. These findings combined with the lower background of the biotinylated hJAA-F11 H2aL2a of IHC normal tissues suggest that hJAA-F11 H2aL2a or other humanized constructs of JAA-F11 are strong candidates for both theranostic and therapeutic uses.

Conclusion

In conclusion, this study highlights the therapeutic potential of JAA-F11 and its humanized derivative, hJAA-F11 H2aL2a, through broad tumor specificity analysis by IHC and radioimmunolocalization in breast and lung tumors in mouse models. Other studies are underway for the preclinical analysis of humanized anti–TF-Ag antibodies supporting their use in direct immunotherapy, antibody-drug conjugate therapy, or bispecific applications as well as in theranostic uses across a wide array of cancers reactive for JAA-F11. JAA-F11 and humanized variants hold great promise with reactivity with 85% of 1269 cases of breast, lung, prostate, colon, ovarian, and bladder cancers. This pancarcinoma reactivity is especially important for cancers with a large unmet need such as TNBC as well as lung cancers. With such a high degree of reactivity in different tumor types, prescreening prior to treatment may not be necessary, but if desired, a multistep theranostic approach, with IHC analysis of tumor binding followed by imaging, could help determine *in vivo* targeting prior to immunotherapy or antibody drug conjugate therapy.

Supplementary data to this article can be found online at https://doi.org/10.1016/j.tranon.2018.01.008.

Competing interests

K. R. O. owns the company, For-Robin Inc., which has licensed the JAA-F11 and hJAA-F11 antibodies from the University at Buffalo.

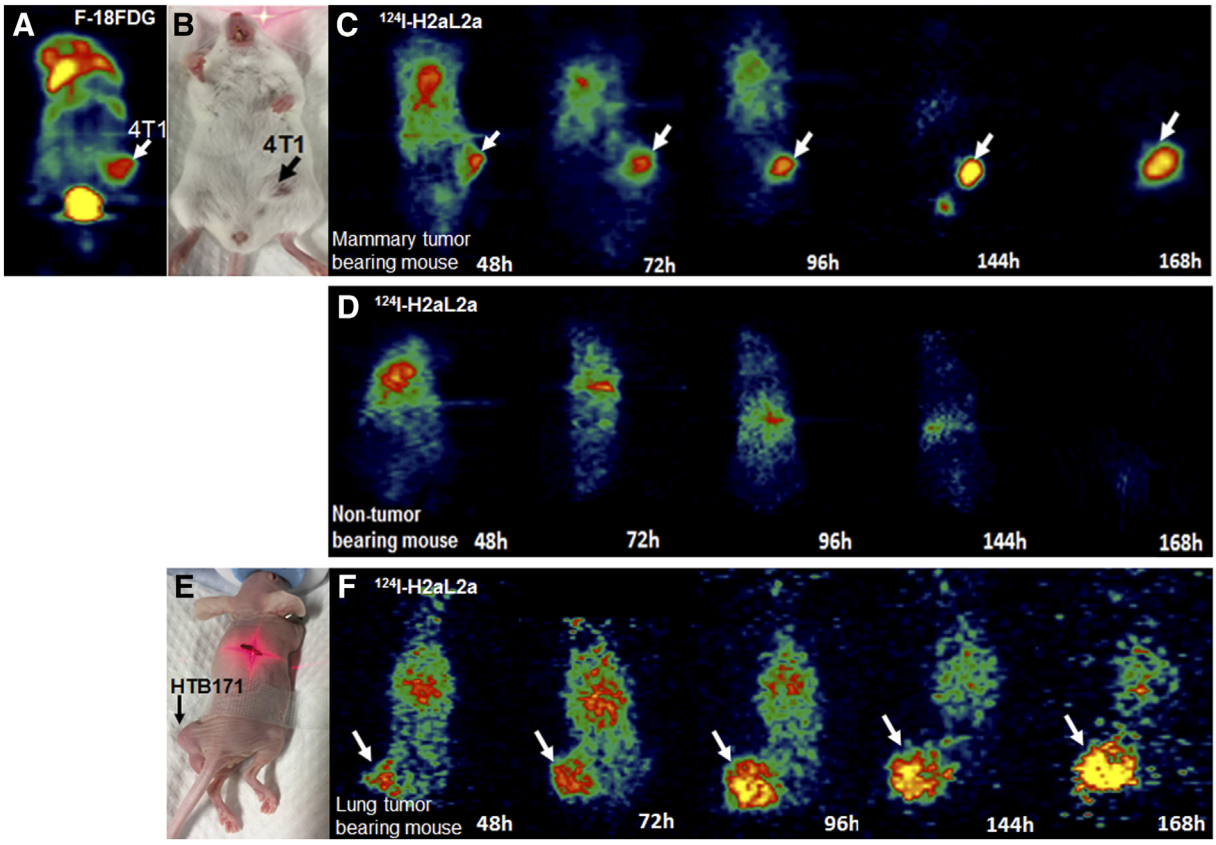

Figure 12. micro-PET immunolocalization of hJAA-F11 H2aL2a in murine models of breast and lung cancers. Representative coronal plane microPET ^{18}F-FDG images (A) were obtained 1 hour postinjection (first column) in Balb/c mice containing 4T1 mammary tumor (B). Representative coronal plane micro-PET scans (tracer is ^{124}I- hJAA-F11 H2aL2a) of Balb/c mice either in the presence (C) or absence (D) of 4T1 mammary tumors. Representative coronal plane micro-PET scans (tracer is ^{124}I hJAA-F11 H2aL2a) (F) of nude mice containing HTB-171 human lung tumor xenografts (E). Tumor indicated by arrow (C, F). The hot spot above the tumor in early time points is the blood pool circulating antibody that is in the heart. This is supported by quantitative biodistribution analysis of blood in the "C" group that found 12.2% of the injected dose remained in each ml of blood at 72 hours, 8.3% per ml of blood at 96 hours, and 0.18% per ml of blood at 168 hours (Figure 13).

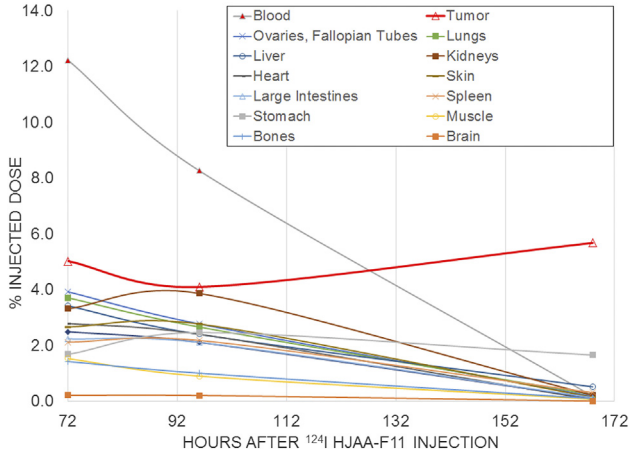

Figure 13. Biodistribution of ^{124}I hJAA-F11 H2aL2a in murine model of breast cancer. Following imaging in Figure 12, mice were sacrificed, indicated organs and tumors were weighed, and the amount of radioactivity was quantified in a gamma-counter with appropriate calibration. Radioactivity uptake was calculated as the percentage of the injected dose per gram of tissue (%ID/g). The total administered radioactivity was determined by measuring the syringes before and after injection with a CRC-12R dose calibrator. The percentage of injected dose (%ID) was corrected utilizing two accompanying standards at the time of each biodistribution analysis.

The University at Buffalo and K. R. O. have the patent for the mouse antibody. K. R. O. does not receive any salary or remuneration from the company at this time or at any time in the past. The University of Buffalo and K. R. O. have applied for a patent for the humanized antibody. Except where noted, there are no other competing interests for any of the authors.

Author Contributions

L. K., J. F., J. J., R. L., and J. A. were involved in the design and performed all the immunohistochemistry experiments. Scoring of IHC slides was done by K. R. O., J. J., and J. R. O. with independent scoring performed by B. T. S. T., D. G., H. J., and M. S. performed the antibody iodination and animal experiments with assistance from S. K. R. R. synthesized the TF-Ag-BSA used. L. K., J. F., S. T., J. R. O., and K. R. O. all prepared and edited the draft of the manuscript. K. R. O. conceived of this study and participated in its design and coordination. All authors read and approved the final manuscript.

Acknowledgements

The authors would like to acknowledge National Institutes of Health STTR grants 1 R41 CA176951-01 (K.R.O.) and 2 R42 CA176951-02A1 (K.R.O.) Clinical Translation of an Anti-Metastatic Antibody for Breast Cancer Therapy. The authors would also like to thank Dr. Sally Quataert at the University at Rochester for her considerable help with editing of the manuscript.

References

[1] MacLean GD, Bowen-Yacyshyn MB, Samuel J, Meikle A, Stuart G, Nation J, Poppema S, Jerry M, Koganty R, and Wong T (1992). Active immunization of human ovarian cancer patients against a common carcinoma (Thomsen-Friedenreich) determinant using a synthetic carbohydrate antigen. *J Immunother (1991)* **11**, 292–305.

[2] Langkilde NC, Wolf H, Clausen H, Kjeldsen T, and Orntoft TF (1992). Nuclear volume and expression of T-antigen, sialosyl-Tn-antigen, and Tn-antigen in carcinoma of the human bladder. Relation to tumor recurrence and progression. *Cancer* **69**, 219–227.

[3] Shamsuddin AM, Tyner GT, and Yang GY (1995). Common expression of the tumor marker D-galactose-beta- 1–>3 -N-acetyl-D-galactosamine by different adenocarcinomas: evidence of field effect phenomenon. *Cancer Res* **55**, 149–152.

[4] Singh R, Campbell BJ, Yu LG, Fernig DG, Milton JD, Goodlad R, FitzGerald AJ, and Rhodes JM (2001). Cell surface-expressed Thomsen-Friedenreich antigen in colon cancer is predominantly carried on high molecular weight splice variants of CD44. *Glycobiology* **11**, 587–592.

[5] Yu LG (2007). The oncofetal Thomsen-Friedenreich carbohydrate antigen in cancer progression. *Glycoconj J* **24**, 411–420.

[6] Cazet A, Julien S, Bobowski M, Burchell J, and Delannoy P (2010). Tumour-associated carbohydrate antigens in breast cancer. *Breast Cancer Res* **12**, 204.

[7] Heimburg-Molinaro J, Lum M, Vijay G, Jain MT, Almogren A, and Rittenhouse-Olson K (2011). Cancer vaccines and carbohydrate epitopes. *Vaccine* **29**, 8802–8826.

[8] Almogren A, Abdullah J, Ghapure K, Ferguson K, Glinsky VV, and Rittenhouse-Olson K (2012). Anti-Thomsen-Friedenreich-Ag (anti-TF-Ag) potential for cancer therapy. *Front Biosci* **4**, 840–863.

[9] Varki A and Freeze HH (2009). Glycans in Acquired Human Diseases. In: Varki A, Cummings RD, Esko JD, Freeze HH, Stanley P, Bertozzi CR, Hart GW, Etzler ME, editors. Essentials of Glycobiology. 2nd ed; 2009 [Cold Spring Harbor (NY). pp].

[10] Ju T, Otto VI, and Cummings RD (2011). The Tn antigen-structural simplicity and biological complexity. *Angew Chem Int Ed Engl* **50**, 1770–1791.

[11] Desai PR (2000). Immunoreactive T and Tn antigens in malignancy: role in carcinoma diagnosis, prognosis, and immunotherapy. *Transfus Med Rev* **14**, 312–325.

[12] Ferguson K, Yadav A, Morey S, Abdullah J, Hrysenko G, Eng JY, Sajjad M, Koury S, and Rittenhouse-Olson K (2014). Preclinical studies with JAA-F11 anti–Thomsen-Friedenreich monoclonal antibody for human breast cancer. *Future Oncol* **10**, 385–399.

[13] Chaturvedi R, Heimburg J, Yan J, Koury S, Sajjad M, Abdel-Nabi HH, and Rittenhouse-Olson K (2008). Tumor immunolocalization using I-124-iodine-labeled JAA-F11 antibody to Thomsen-Friedenreich alpha-linked antigen. *Appl Radiat Isot* **66**, 278–287.

[14] Glinsky VV, Glinsky GV, Rittenhouse-Olson K, Huflejt ME, Glinskii OV, Deutscher SL, and Quinn TP (2001). The role of Thomsen-Friedenreich antigen in adhesion of human breast and prostate cancer cells to the endothelium. *Cancer Res* **61**, 4851–4857.

[15] Khaldoyanidi SK, Glinsky VV, Sikora L, Glinskii AB, Mossine VV, Quinn TP, Glinsky GV, and Sriramarao P (2003). MDA-MB-435 human breast carcinoma cell homo- and heterotypic adhesion under flow conditions is mediated in part by Thomsen-Friedenreich antigen-galectin-3 interactions. *J Biol Chem* **278**, 4127–4134.

[16] Zou J, Glinsky VV, Landon LA, Matthews L, and Deutscher SL (2005). Peptides specific to the galectin-3 carbohydrate recognition domain inhibit metastasis-associated cancer cell adhesion. *Carcinogenesis* **26**, 309–318.

[17] Heimburg J, Yan J, Morey S, Glinskii OV, Huxley VH, Wild L, Klick R, Roy R, Glinsky VV, and Rittenhouse-Olson K (2006). Inhibition of spontaneous breast cancer metastasis by anti-Thomsen-Friedenreich antigen monoclonal antibody JAA-F11. *Neoplasia* **8**, 939–948.

[18] Glinskii OV, Sud S, Mossine VV, Mawhinney TP, Anthony DC, Glinsky GV, Pienta KJ, and Glinsky VV (2012). Inhibition of prostate cancer bone metastasis by synthetic TF antigen mimic/galectin-3 inhibitor lactulose-L-leucine. *Neoplasia* **14**, 65–73.

[19] Glinskii OV, Li F, Wilson LS, Barnes S, Rittenhouse-Olson K, Barchi Jr JJ, Pienta KJ, and Glinsky VV (2014). Endothelial integrin alpha3beta1 stabilizes carbohydrate-mediated tumor/endothelial cell adhesion and induces macromolecular signaling complex formation at the endothelial cell membrane. *Oncotarget* **5**, 1382–1389.

[20] Uhlenbruck G, Pardoe GI, and Bird GW (1969). On the specificity of lectins with a broad agglutination spectrum. II. Studies on the nature of the T-antigen and the specific receptors for the lectin of Arachis hypogoea (ground-nut). *Z Immunitatsforsch Allerg Klin Immunol* **138**, 423–433.

[21] Lotan R, Skutelsky E, Danon D, and Sharon N (1975). The purification, composition, and specificity of the anti-T lectin from peanut (Arachis hypogaea). *J Biol Chem* **250**, 8518–8523.

[22] Springer GF (1997). Immunoreactive T and Tn epitopes in cancer diagnosis, prognosis, and immunotherapy. *J Mol Med* **75**, 594–602.

[23] Cao Y, Stosiek P, Springer GF, and Karsten U (1996). Thomsen-Friedenreich-related carbohydrate antigens in normal adult human tissues: a systematic and comparative study. *Histochem Cell Biol* **106**, 197–207.

[24] Hanisch FG and Baldus SE (1997). The Thomsen-Friedenreich (TF) antigen: a critical review on the structural, biosynthetic and histochemical aspects of a pancarcinoma-associated antigen. *Histol Histopathol* **12**, 263–281.

[25] Tang H, Hsueh P, Kletter D, Bern M, and Haab B (2015). The detection and discovery of glycan motifs in biological samples using lectins and antibodies: new methods and opportunities. *Adv Cancer Res* **126**, 167–202.

[26] Neurohr KJ, Bundle DR, Young NM, and Mantsch HH (1982). Binding of disaccharides by peanut agglutinin as studied by ultraviolet difference spectroscopy. *Eur J Biochem* **123**, 305–310.

[27] Haines DM (1993). Peanut agglutinin lectin immunohistochemical staining of normal and neoplastic canine tissues. *Vet Pathol* **30**, 333–342.

[28] Rahman AF and Longenecker BM (1982). A monoclonal antibody specific for the Thomsen-Friedenreich cryptic T antigen. *J Immunol* **129**, 2021–2024.

[29] Longenecker BM, Willans DJ, MacLean GD, Selvaraj S, Suresh MR, and Noujaim AA (1987). Monoclonal antibodies and synthetic tumor-associated glycoconjugates in the study of the expression of Thomsen-Friedenreich-like and Tn-like antigens on human cancers. *J Natl Cancer Inst* **78**, 489–496.

[30] Karsten U, Butschak G, Cao Y, Goletz S, and Hanisch FG (1995). A new monoclonal antibody (A78-G/A7) to the Thomsen-Friedenreich pan-tumor antigen. *Hybridoma* **14**, 37–44.

[31] Clausen H, Stroud M, Parker J, Springer G, and Hakomori S (1988). Monoclonal antibodies directed to the blood group A associated structure, galactosyl-A: specificity and relation to the Thomsen-Friedenreich antigen. *Mol Immunol* **25**, 199–204.

[32] Mahanta SK, Sastry MV, and Surolia A (1990). Topography of the combining region of a Thomsen-Friedenreich-antigen-specific lectin jacalin (Artocarpus integrifolia agglutinin). A thermodynamic and circular-dichroism spectroscopic study. *Biochem J* **265**, 831–840.

[33] Hanisch FG, Stadie T, and Bosslet K (1995). Monoclonal antibody BW835 defines a site-specific Thomsen-Friedenreich disaccharide linked to threonine within the VTSA motif of MUC1 tandem repeats. *Cancer Res* **55**, 4036–4040.

[34] Wang BL, Springer GF, and Carlstedt SC (1997). Quantitative computerized image analysis of Tn and T (Thomsen-Friedenreich) epitopes in prognostication of human breast carcinoma. *J Histochem Cytochem* **45**, 1393–1400.

[35] Baldus SE, Hanisch FG, Kotlarek GM, Zirbes TK, Thiele J, Isenberg J, Karsten UR, Devine PL, and Dienes HP (1998). Coexpression of MUC1 mucin peptide core and the Thomsen-Friedenreich antigen in colorectal neoplasms. *Cancer* **82**, 1019–1027.

[36] Dahlenborg K, Hultman L, Carlsson R, and Jansson B (1997). Human monoclonal antibodies specific for the tumour associated Thomsen-Friedenreich antigen. *Int J Cancer* **70**, 63–71.

[37] Tati S, Fisk JC, Abdullah J, Karacosta L, Chrisikos T, Philbin P, Morey S, Ghazal D, Zalzala F, and Jessee J, et al (2017). Humanization of JAA-F11, a highly specific anti–Thomsen-Friedenreich pancarcinoma antibody and in vitro efficacy analysis. *Neoplasia* **19**, 716–733.

[38] Biomax U (2017). US Biomax, Inc FAQs; 2017.

[39] Rittenhouse-Diakun K, Xia Z, Pickhardt D, Morey S, Baek MG, and Roy R (1998). Development and characterization of monoclonal antibody to T-antigen: (gal beta1-3GalNAc-alpha-O). *Hybridoma* **17**, 165–173.

[40] Collingridge DR, Carroll VA, Glaser M, Aboagye EO, Osman S, Hutchinson OC, Barthel H, Luthra SK, Brady F, and Bicknell R, et al (2002). The development of [(124)I]iodinated-VG76e: a novel tracer for imaging vascular endothelial growth factor in vivo using positron emission tomography. *Cancer Res* **62**, 5912–5919.

[41] Chaturvedi R (2006). Tumor immunolocalization using iodine-124 radiolabeled monoclonal antibody JAA-F11. University at Buffalo Thesis; 2006.

[42] Glinskii OV, Huxley VH, Glinsky GV, Pienta KJ, Raz A, and Glinsky VV (2005). Mechanical entrapment is insufficient and intercellular adhesion is essential for metastatic cell arrest in distant organs. *Neoplasia* **7**, 522–527.

[43] Li F, Glinskii OV, Mooney BP, Rittenhouse-Olson K, Pienta KJ, and Glinsky VV (2017). Cell surface Thomsen-Friedenreich proteome profiling of metastatic prostate cancer cells reveals potential link with cancer stemcell-like phenotype. *Oncotarget.* **8**, 98598–98608.

[44] Glinskii OV, Turk JR, Pienta KJ, Huxley VH, and Glinsky VV (2004). Evidence of porcine and human endothelium activation by cancer-associated carbohydrates expressed on glycoproteins and tumour cells. *J Physiol* **554**, 89–99.

[45] Gassmann P, Kang M-L, Mees ST, and Haier J (2010). In vivo tumor cell adhesion in the pulmonary microvasculature is exclusively mediated by tumor cell-endothelial cell interaction. *BMC Cancer* **10**, 177.

[46] Goletz S, Cao Y, Danielczyk A, Ravn P, Schoeber U, and Karsten U (2003). Thomsen-Friedenreich antigen: the "hidden" tumor antigen. *Adv Exp Med Biol* **535**, 147–162.

[47] Imai J, Ghazizadeh M, Naito Z, and Asano G (2001). Immunohistochemical expression of T, Tn and sialyl-Tn antigens and clinical outcome in human breast carcinoma. *Anticancer Res* **21**, 1327–1334.

[48] Cao Y, Karsten U, Otto G, and Bannasch P (1999). Expression of MUC1, Thomsen-Friedenreich antigen, Tn, sialosyl-Tn, and alpha2,6-linked sialic acid in hepatocellular carcinomas and preneoplastic hepatocellular lesions. *Virchows Arch* **434**, 503–509.

[49] Cao Y, Karsten UR, Liebrich W, Haensch W, Springer GF, and Schlag PM (1995). Expression of Thomsen-Friedenreich-related antigens in primary and metastatic colorectal carcinomas. A reevaluation. *Cancer* **76**, 1700–1708.

[50] Cao Y, Merling A, Karsten U, Goletz S, Punzel M, Kraft R, Butschak G, and Schwartz-Albiez R (2008). Expression of CD175 (Tn), CD175s (sialosyl-Tn) and CD176 (Thomsen-Friedenreich antigen) on malignant human hematopoietic cells. *Int J Cancer* **123**, 89–99.

[51] Siegel RL, Miller KD, and Jemal A (2017). Cancer statistics, 2017. *CA Cancer J Clin* **67**, 7–30.

[52] Heimburg-Molinaro J and Rittenhouse-Olson K (2009). Development and Characterization of Antibodies to Carbohydrate Antigens. In: Packer NH, Karlsson NG, editors. Glycomics. Methods in Molecular Biology™ (Methods and Protocols), vol 534. Totowa, NJ: Humana Press; 2009.

[53] Cheal SM, Punzalan B, Doran MG, Evans MJ, Osborne JR, Lewis JS, Zanzonico P, and Larson SM (2014). Pairwise comparison of 89Zr- and 124I-labeled cG250 based on positron emission tomography imaging and nonlinear immunokinetic modeling: in vivo carbonic anhydrase IX receptor binding and internalization in mouse xenografts of clear-cell renal cell carcinoma. *Eur J Nucl Med Mol Imaging* **41**, 985–994.

[54] Fonge H and Leyton JV (2013). Positron emission tomographic imaging of iodine 124 anti-prostate stem cell antigen-engineered antibody fragments in LAPC-9 tumor-bearing severe combined immunodeficiency mice. *Mol Imaging* **12**, 191–202.

[55] Burvenich I, Schoonooghe S, Cornelissen B, Blanckaert P, Coene E, Cuvelier C, Mertens N, and Slegers G (2005). In vitro and In vivo targeting properties of iodine-123- or iodine-131–labeled monoclonal antibody 14C5 in a non–small cell lung cancer and colon carcinoma model. *Clin Cancer Res* **11**, 7288–7296.

[56] Springer GF, Desai PR, and Banatwala I (1974). Blood group MN specific substances and precursors in normal and malignant human breast tissues. *Naturwissenschaften* **61**, 457–458.

[57] McQuarrie SA, MacLean GD, Boniface GR, Golberg K, and McEwan AJ (1997). Radioimmunoscintigraphy in patients with breast adenocarcinoma using technetium-99m labelled monoclonal antibody 170H.82: report of a phase II study. *Eur J Nucl Med* **24**, 381–389.

[58] Lehmann J, DeNardo GL, Yuan A, Shen S, O'Donnell RT, Richman CM, and DeNardo SJ (2006). Comparison of normal tissue pharmacokinetics with 111In/90Y monoclonal antibody m170 for breast and prostate cancer. *Int J Radiat Oncol Biol Phys* **66**, 1192–1198.

[59] Abdi EA, Kamitomo VJ, McPherson TA, Catz Z, Boniface G, Longenecker BM, and Noujaim AA (1986). Radioiodinated peanut lectin: clinical use as a tumour-imaging agent and potential use in assessing renal-tubular function. *Eur J Nucl Med* **11**, 350–354.

[60] Philipsen EK, Jorgensen M, and Dabelsteen E (1991). Expression of blood group-related carbohydrate antigens in normal human pancreatic tissue. *APMIS* **99**, 931–940.

[61] Cocariu EA, Mageriu V, Staniceanu F, Bastian A, Socoliuc C, and Zurac S (2016). Correlations between the autolytic changes and postmortem interval in refrigerated cadavers. *Rom J Intern Med* **54**, 105–112.

[62] Monti E, Preti A, Venerando B, and Borsani G (2002). Recent development in mammalian sialidase molecular biology. *Neurochem Res* **27**, 649–663.

[63] Goswami C, Kuhn J, Dina OA, Fernandez-Ballester G, Levine JD, Ferrer-Montiel A, and Hucho T (2011). Estrogen destabilizes microtubules through an ion-conductivity-independent TRPV1 pathway. *J Neurochem* **117**, 995–1008.

[64] Holtzer RL and van Lancker JL (1962). Early changes in pancreas autolysis. *Am J Pathol* **40**, 331–336.

[65] Presnell SE (2015). Postmortem changes. *Medscape* **2015**.

[66] Van Lancker JL and Holtzer RL (1959). The Release of acid phosphatase and beta-glucuronidase from cytoplasmic granules in the early course of autolysis. *Am J Pathol* **35**, 563–573.

[67] Goodpaster T and Randolph-Habecker J (2014). A flexible mouse-on-mouse immunohistochemical staining technique adaptable to biotin-free reagents, immunofluorescence, and multiple antibody staining. *J Histochem Cytochem* **62**, 197–204.

[68] Schwartz AL, Marshak-Rothstein A, Rup D, and Lodish HF (1981). Identification and quantification of the rat hepatocyte asialoglycoprotein receptor. *Proc Natl Acad Sci U S A* **78**, 3348–3352.

[69] Tessier MB, Grant OC, Heimburg-Molinaro J, Smith D, Jadey S, Gulick AM, Glushka J, Deutscher SL, Rittenhouse-Olson K, and Woods RJ (2013). Computational screening of the human TF-glycome provides a structural definition for the specificity of anti-tumor antibody JAA-F11. *PLoS One* **8**, e54874.